Dear Editor:

Thank you very much for your attention and the referee's evaluation and comments on our paper "Second-order Scalar Wave Field Modeling with First-order Perfectly Matched Layer" (ID: se-2018-48). Based on referee's comment and request, we have made extensive modification on the original manuscript. Enclosed please find the responses to the referees and the marked-up manuscript. We sincerely hope this manuscript will be finally acceptable to be published on "Solid Earth". Thank you very much for all your help and looking forward to hearing from you soon.

Best regards

Sincerely yours

Xiaoyu Zhang

Response to the referee's comments (The number of Line and Page given in the comments and Responses is related to the revised manuscript, not the marked-up manuscript.):

Referee 1:

Major comments:

1. Comment: In general, it's a bit hard to follow the description of the algorithm (Page 8). Maybe it's helpful to zoom in Fig 1 and label more symbols in the figure that are used in the text, e.g. $p_x^n(i_r, j_r)$, $v_x^{n+\frac{1}{2}}\left(i_r + \frac{1}{2}, j_r\right)$, etc. Also, please mention the updated $p_{i,j}^{n+1}$ in Step 2 is not used in Step 3, in which the old $p_{i,j}^n$ value is used to calculate $v_x^{n+\frac{1}{2}}\left(i + \frac{1}{2}, j\right)$ and $v_z^{n+\frac{1}{2}}\left(i, j + \frac{1}{2}\right)$ and therefore requires storing these old $p_{i,j}^n$ values on the red lines, the cost of which is however negligible.

Response: Thanks for the referee's suggestion. The schematic of our method is too general for understanding. So we have zoomed in Fig. 1 and labeled more symbols in the Fig. 1(b) (Page 7) that are used in the text. Meanwhile, the updated $p_{i,j}^{n+1}$ in the Step 2 is indeed not used in Step 3. However, only for the calculation of $v_x^{n+\frac{1}{2}}\left(i + \frac{1}{2}, j\right)$ and $v_z^{n+\frac{1}{2}}\left(i, j + \frac{1}{2}\right)$ in the overlapping area between the computational area and PML area, do we need to use the old $p_{i,j}^n$ values on the red lines. For the conventional-grid finite-difference scheme, the discretization of acoustic wave equation with a 2*M*-order finite-difference scheme is

$$p_{i,j,k}^{n+1} = 2p_{i,j,k}^n - p_{i,j,k}^{n-1} + \frac{c^2 \Delta t^2}{\Delta x^2}\left[c_0 p_{i,j,k}^n + \sum_{m=1}^{M} c_m\left(p_{i-m,j,k}^n + p_{i+m,j,k}^n\right)\right]$$

$+ \frac{c^2 \Delta t^2}{\Delta y^2}[c_0 p_{i,j,k}^n + \sum_{m=1}^{M} c_m(p_{i,j-m,k}^n + p_{i,j+m,k}^n)] + \frac{c^2 \Delta t^2}{\Delta z^2}[c_0 p_{i,j,k}^n + \sum_{m=1}^{M} c_m(p_{i,j,k-m}^n +$

$p_{i,j,k+m}^n)]$.

So in the computational area, we have to temporarily store the old $p_{i,j}^n$ values. This will increase some storage capacity, but for staggered-grid, the total computational capacity is still saved. At the same time, the use of the second-order difference of time can also increase the calculation accuracy. The red lines are the boundary lines of the computational area, we have already stored the $p_{i,j}^n$ in

the previous calculation.

2. Comment: For the algorithm, I think author just show the case when 2nd-order finite-difference is used for discretization in space. Please give a clear description in the paper as your first numerical example has shown that a reasonably accurate modeling (i.e. no strong dispersion) requires at least the 4th-order finite-difference approximation.

Response: It was our carelessness that we did not give a clear description if higher-orders were used in the computational area. In actual processing, one of our goals is to keep the computational area and PML area independent. In the computational area, we reduce the order of difference on the boundary layer by layer. We have redrawn the Fig. 1 on the Page 7 as Fig. 1(a). For the high-order difference scheme in the computational area, we use the second-order difference scheme for the grid points on the blue rectangular line, the fourth-order difference scheme for the grid points on the inner green rectangular line, and the sixth-order difference scheme on the inner layer, and so on, until we reach the required order of difference. In this way, the number of overlapping layers does not increase with the increase of order of difference in the computational area. The results of numerical experiments in Fig. 3-10 show that our treatment to the boundary does not bring much additional dispersion and error.

3. Comment: In Section 4.2, the 2nd-order PML (e.g., third columns of Fig. 15) behaves quite poorer than the two methods mentioned before. Why does this occur? Although the realization is different, the 2nd-order PML borrows the same idea as the 1st-order PML and thus they should have similar behavior. In addition, why is the hybrid ABC method the worst of all?

Response: Although the core idea of the second-order PML method is the same as the first-order PML method, there are very different ways to deal with mathematical equations. In the second-order method, the original PML equations are transformed and some additional nonphysical variables are added, which greatly reduce the efficiency of boundary conditions. Moreover, the second-order PML method still need to handle the first-order system, i.e. an Euler or a Runge-Kutta time scheme has to be used (Komatitsch and Tromp, 2003). So in this case, the second-order PML method is naturally less effective than our first-order PML method and requires more absorbing layers, which is consistent with the numerical experimental results in Section 4.2. Our method only requires a thickness of 10 layers to absorb the outgoing wave entirely, while the second-order PML method requires 20 or more. This may be one of a significant advantages over the second-order PML method. For hybrid ABC, it has poor absorbing performance than the PML method since it is based on a one-way equation. So it would have limited improvement due to the phase and the amplitude errors that are associated with the expansion of one-way wave equation (Gao et al., 2017).

In order to make the interpretation of the experimental results clearer, I added this explanation in Section 4.2 in Line 14-22, Page 23.

4. Comment: I would suggest the authors also compare the proposed method with the C-PML method because it has been shown better absorbing capability than the classical PML especially at grazing angles (Komatitsch and Martin, 2007).

Response: In numerical experiments, we compare the absorption effects of four method: our method, the classic PML method, the second-order PML method, and the hybrid ABC method. We choose the second-order PML method for comparison in order to prove the superiority of the first-

order PML system and we choose the hybrid ABC method because many scholars prefer to use the hybrid ABC method when adopting the conventional-grid in the computational area. We choose the classic PML method because it is more commonly used in real seismic simulation. As another first-order PML method, C-PML method is indeed an excellent method. However, the main purpose of our paper is to combine the first-order PML system and the second-order wave equation system, so that the boundary absorption effect can be the same good as the first-order PML with the first-order wave equation so that the computational efficiency can be greatly increased. Comparing the absorption effects of different first-order PML methods is not our goal, and there are many papers that have done similar work. Gao et al. (2017) did many numerical experiments and concluded that the 10-layer PML is accurate enough when the nearly grazing wave is not serious and the 20-layer PML is suggested for most practical applications for general size models, even in the presence of strong nearly grazing waves, while the 20-layer C-PML is only necessary when the source is located fairly close to the boundary for large-scale models, where the nearly grazing wave is severe. Moreover, the C-PML method is often used in the boundary treatment of staggered-grid, which is the same as the classic PML method. If our method can correctly deal with the matching problem between the classic PML method and the conventional-grid, it can also deal with the matching problem between the C-PML method and the conventional-grids. Thanks for the referee's advice, which led us to discover more possibilities for our work. We will consider this situation in future work.

Minor comments:

1. Comment: The sentence in Line 6, Page 3 is vague: how to eliminate, which modeling algorithm? The information is not clearly delivered by this sentence neither from the context. I would suggest just remove this sentence.

   Response: I was going to express that the reflection error could be eliminated by different boundary absorption method. This expression is not appropriate here, so I have removed this sentence.

2. Comment: Throughout the paper, please use a period after an equation to finalize the sentence, or a comma if it is followed by "where" (continuation of the sentence).

   Response: Thanks for pointing out this error. I have added commas or periods after all the equations.

3. Comment: Throughout the paper, you can attach a number to each line of the equations, see Line 11-17, Page 5.

   Response: Thanks for pointing out the problem of labeling sentences. I think the seven equations here can be seen as a joint formula, so one label is enough.

4. Comment: For $p_x^n(i_r, j_r)$ and p_{i_b, j_b}^n in Line 14, Page 8, help understanding the meaning of "r" and "b".

   Response: I was sorry I ignored the meaning of this subscript. The subscript r stands for the grid points on the red lines, and b stands for the blue lines. The explanation has been added in Line 16-17, Page 8.

5. Comment: For the sentence "For the two-dimensional scalar equation (1), the wave field analytic solution for a homogeneous medium can be obtained from…" in Line 17, Page 9, I think you mean a "constant-gradient" medium here.

  Response: I was sorry that I made a mistake. It should be "constant-gradient" here. I have corrected it in Line 17, Page 9.

6. Comment: In Line 20, Page 9, what is "h" in $\gamma = \frac{1}{h}$?

  Response: h is the distance from depth z=0 to the level where the propagation velocity is null (c(-h)=0). The explanation has been added in Line 21, Page 9

7. Comment: In Line 28, Page 9, the "arecosh" in the equation should be "arccosh".

  Response: Thanks for pointing out this mistake in writing. It has been corrected in Line 28, Page 9.

8. Comment: In equation 13 (Line 9, Page 10), it's better to write "t" below "max" to indicate the maximum value is selected within a trace.

  Response: I am sorry I do not understand the meaning of "within a trace" here. The "max" I put in this equation means the maximum value of the value $p(t) - p_{ref}(t)$ or the wave field value $p_{ref}(t)$ during the total simulation time. So I do not change anything here.

9. Comment: In Fig. 12, 15, 18, please use same spacing of ticks in the panels. If not, we don't know where the 0th, 50th, 100th, 150th, 200th receivers are in the rest three panels.

  Response: Thanks for pointing out the error of panel spacing. It has been corrected.

10. Comment: To be persuasive, this claim (Line 13, Page 23) would need a reference to another work illustrating the same behavior.

  Response: I have added some explanation and related reference in Line 14-22, Page 23. These can explain why the second-order PML method always requires more absorbing layers than the first-order PML does.

Referee 2:

1. Comment: There are some spelling errors and misuse of words, especially in the introduction and conclusion, which need correction.

  Response: Thanks for this suggestion. The spelling errors and misuse of words have been checked and corrected.

2. Comment: There is no hyphen in the "staggered-grid" and "conventional-grid".

  Response: Thanks for the referee's careful reading of our manuscript. I think two kinds of writing are both acceptable. I prefer to use "staggered-grid" and "conventional-grid".

3. Comment: The paragraph from the Line 15, Page 2 is too long. Make it into two

  Response: This paragraph is composed of two parts. The first part describes the development of the staggered-grid and conventional-grid. The second part describes their respective advantages and

disadvantages and related literature. So I divide the paragraph into two from Line 28, Page 2.

4. Comment: what's the meaning of j in equation 4 (Line 20, Page 5)?

Response: P_{ml} is the thickness of the PML layer, j is the number of layers from the computational area boundary.

5. Comment: In Fig. 1(a) on Page 7, will it be better if the space between blue line and red line is thicker? In other words, is one layer of grids enough?

Response: In our method, on the one hand, if higher-order difference is used in the computational area, the order of difference will be reduced layer by layer from the boundary of computational area to the center. As abovementioned in the response to Major comment 2 of referee 1, we have redrawn the Fig. 1 on the Page 7 as Fig. 1(a). For the high-order difference scheme in the computational area, we use the second-order difference scheme for the grid points on the blue rectangular line, the fourth-order difference scheme for the grid points on the inner green rectangular line, and the sixth-order difference scheme on the inner layer, and so on, until we reach the required order of difference. In this way, we only need one overlapping layer to exchange the pressure field between the PML area and the inner computational area. On the other hand, if we use higher-order difference in PML area, we will indeed need more than one overlapping layer. However, generally speaking, high-order difference is seldom used in the PML area, and the first-order difference can completely achieve the desired absorption effect. Therefore, in our method, the use of one layer of grids is enough. In future work, we can further discuss the use of high-order difference in PML area.

6. Comment: In step 3 of the proposed method (Line 8, Page 8), does the calculation order of grids have to be from left to right and from top to bottom? Can it be from inside to outside?

Response: The calculation order of grids is arbitrary. It can be calculated from left to right and from top to bottom or from inside to outside. So I just deleted this sentence.

7. Comment: Explain what i_r and j_r mean in $p_x^n(i_r, j_r)$ and p_{i_b, j_b}^n in Line 15, Page 8.

Response: I was sorry I ignored the meaning of this subscript. As abovementioned in the response to Minor comment 4 of referee 1, the subscript r stands for the grid points on the red lines, and b stands for the blue lines. The explanation has been added in Line 16-17, Page 8.

8. Comment: what is the goal of this sentence in Line 24-26, Page 8?

Response: The red line is both the outermost boundary of the computational area and the innermost boundary of the PML area. When this line acts as the boundary of PML area, the value of wave field are represented by $p_x^{n+1}(i_r, j_r)$ and $p_z^{n+1}(i_r, j_r)$; when it acts as the boundary of computational area, the value of wave field are represented by $p_{i,j}^{n+1}$. $p_x^{n+1}(i_r, j_r)$ and $p_z^{n+1}(i_r, j_r)$, and $p_{i,j}^{n+1}$ actually refer to the same point, so here we make the value of them equal:
$$p_{i,j}^{n+1} = p_x^{n+1}(i_r, j_r) + p_z^{n+1}(i_r, j_r).$$

9. Comment: what does "h" mean in $\gamma = 1/h$ in Line 20, Page 9?

Response: As abovementioned in the response to Minor comment 6 of referee 1, h is the distance from depth z=0 to the level where the propagation velocity is null (c (-h) =0). The explanation has been added in Line 21, Page 9

10. Comment: Can you find references of exact analytic solution? (Equation 11 in Line 24, Page 9)

Response: I'm very sorry that we haven't found references of exact analytic solution here. In the Section 3.1, we gave the approximate analytical solution of constant-gradient medium, which is derived from the homogeneous medium. For two-dimensional homogeneous medium, there is exact analytical solution:

$$G(x, z, t) = \frac{H(t - t_0 - \tau)}{2\pi\sqrt{(t - t_0)^2 - \tau^2}}.$$

In order to deduce the solution of constant-gradient medium, we transformed the above equation into frequency domain by Flourier transformation, did some modification and then changed back to time domain. In the modification, we used Hankel's function of the first kind and zero order, and related approximation:

$$H_0^{(1)}\left(\omega \frac{r}{c}\right) \approx \left(\frac{2c}{\pi}\right)^{\frac{1}{2}}\left(\frac{1}{\omega r}\right)^{\frac{1}{2}} \exp(\frac{i\omega r}{c} - \frac{i\pi}{4}).$$

It is the Neumann's asymptotic from of Hankel's function for large $\omega \frac{r}{c}$. This is the only place we used the approximation. This approximation is acceptable and is also adopted in some reference on the accuracy comparison of numerical algorithms (Sanchez-Sesma et al., 2001; Luzón et al., In-plane seismic response of inhomogeneous alluvial valleys with vertical gradients of velocities and constant Poisson ratio. *Soil Dynamics & Earthquake Engineering*, 2009, 29, 994-1004; Fontara et al., Seismic wave fields in continuously inhomogeneous media with variable wave velocity profiles. *Archive of Applied Mechanics*, 2015, 86, 1-24; Ge, Simulation of the seismic response of sedimentary basins with constant-gradient velocity along arbitrary direction using boundary element method: SH case. *Earthquake Science*, 2010, 23, 149-155.).

11. Comment: what is the reason to choose 10m to do the numerical experiments?

Response: Our choice of 10m is determined by the stability and time interval of the differential form, and we find that in some related seismic simulation references, researchers also prefer to use 10m.

12. Comment: Put the 3 kinds of data in a single figure of Fig. 3, 4, 6, 7, 9. And zoom in the figures on the right.

Response: Thank you for pointing out this problem. If we put the three kinds of data together, some of them will be mixed up, especially some numerical oscillation at the end of waveform. So I think it's better to separate them.

13. Comment: Two Lines overlap each other in Fig. 5, 8, 10. Use 6*1 figures to widen the figures. And use less time samples to be sparser.

Response: Thank you for pointing out the problem in the picture. We chose 10 seconds to prove the stability of our method. We have used 3*2 figures to widen the figure and appropriately increased the time interval. After enlargement, we can see that the amplitude of the red line and the blue line is almost the same.

14. Comment: Why say "Of course, these conclusions also apply to other inhomogeneous

mediums."? (Line 15, Page 20)

Response: I'm sorry we shouldn't written this sentence. We think that the constant-gradient medium and other inhomogeneous mediums may have the same law. However, we cannot draw this conclusion without doing the relevant experiments. We have already deleted this sentence.

15. Comment: Section 4.2 should be divided into three parts.

Response: Thanks for pointing this out. I have divided Section 4.2 into three parts: Homogeneous model, Constant-gradient velocity model, and Marmousi model.

16. Comment: The sentence "The model size is 1000 m×1000 m" is wrong. (Line 14, Page 28)

Response: Sorry, the model size should be 1000 m×1000 m×1000 m. I have corrected it.

17. Comment: In Figure 19, what does the 100 here mean?

Response: The 100 here means one hundred grid points. The explanation of the figure have been added in the Line 4, Page 29.

Modifications by ourselves

1. In order to distinguish the wave field value in the computational area and the PML area, we added an explanation sentence "In order to distinguish, we use $p_{i,j}^{n+1}$ to represent the wave field value in the computational area, and $p_x^n(i,j)$ and $p_z^n(i,j)$ to represent the wave field value in the PML area" in Line 22-24, Page 6.

2. In Table 1 in Page 20, we deleted the fifth rows because we didn't do the experiment of tenth-order and d=12m.

3. We gave more description about Fig, 13 in Line 8-10, Page 23.

Marked-up manuscript is attached as following.

Second-order Scalar Wave Field Modeling with First-order Perfectly Matched Layer

Xiaoyu Zhang[1], Dong Zhang[1*], Qiong Chen[1], Yan Yang[1]

[1]School of Physics and Technology, Wuhan University, Wuhan, Hubei, China.

[*]E-mail: dongz@whu.edu.cn

Data of submission 28 May 2018.

Abstract: The forward modeling of a scalar wave equation plays an important role in the numerical geophysical computations. The finite-difference algorithm in the form of a second-order wave equation is one of the commonly used forward numerical algorithms. This algorithm is simple and is easy to implement based on the conventional-grid. In order to ensure the accuracy of the calculation, absorption layers should be introduced around the computational area to suppress the wave reflection caused by the artificial boundary. For boundary absorption conditions, a perfectly matched layer is one of the most effective algorithms. However, the traditional perfectly matched layer algorithm is calculated using a staggered-grid based on the first-order wave equation, which is difficult to directly integrate into a conventional-grid finite-difference algorithm based on the second-order wave equation. Although a perfectly matched layer algorithm based on the second-order equation can be derived, the formula is rather complex and intermediate variables need to be introduced, which makes it hard to implement. In this paper, we present a simple and efficient algorithm to match the variables at the boundaries between the computational area and the absorbing boundary area. This new boundary matched method can integrate the traditional staggered-grid perfectly matched layer algorithm and the conventional-grid finite-difference algorithm without formula transformations, and it can ensure the accuracy of finite-difference forward modeling in the computational area. In order to verify the validity of our method, we used several models to carry out numerical simulation experiments. The comparison between the simulation results of our new boundary matched algorithm and other boundary absorption algorithms shows that our proposed method suppresses the reflection of the artificial boundaries better and has a higher computational efficiency.

Keywords: seismic waves, boundary conditions, absorption, second-order wave equation, conventional-grid.

1 Introduction

Modeling of a seismic wave field is accomplished by simulating the pattern of the seismic waves as they propagate through various geologic media and computing the simulated measurements at observation points on the Earth's surface or underground, given that the underground medium's structure and the relevant physical parameters are known. Numerical modeling of a seismic wave field is an important tool for seismic data processing and interpretation and for geodynamic studies of the Earth's interior. In recent years, many full waveform inversion methods have been widely proposed and applied to seismic exploration. In the waveform inversion process, wave field modeling is one of the key algorithms because it must be performed first to obtain the predicted wave field that is used to compute the residual errors between the predicted and the actual wave

field records. In addition, the information provided by the residual errors, which is required for refinement of the initial model, is actually calculated by a modeling algorithm that uses the residual errors as virtual sources. After many iterations of the above processes, an optimized approximate model of the underground medium can be acquired. Numerical modeling of a wave field will be executed thousands of times throughout the waveform inversion process, so a wave field modeling algorithm is crucial in many ways when performing a waveform inversion algorithm, such as computational precision, speed, and storage requirements.

The main numerical techniques for seismic wave field modeling include the finite-element method (Marfurt, 1984; Yang et al., 2008), the pseudo-spectral method (Kreiss and Oliger, 1972; Dan and Baysal, 1982), and the finite-difference method (Kelly et al., 2012; Virieux, 1984; Yang et al., 2002; Moczo et al., 2007; Zhang et al., 2013). Due to its easy implementation and the satisfactory compromise between accuracy and efficiency, the finite-difference method is the preferred method. For a comprehensive overview of applications of the finite-difference methods, see Moczo et al. (2014). Over the last several decades, many studies have focused on determining the coefficients of the finite-difference method and designing computational templates (Liu et al., 2017).

According to the formulation of the wave equations, the finite-difference methods can be implemented based on the first-order velocity-stress equations or the second-order displacement equations, which lead to different computational templates. A staggered-grid (SG) is usually set up for the first-order wave equations and has been widely used with the acoustic and elastic wave equations (Virieux, 1984; Moczo et al., 2014; Madariaga, 1976; Virieux, 1986; Gold et al.,1997; Saenger et al., 2000; O'Brien, 2010). Many methods of optimizing the differential coefficients, based on a SG, have been proposed to increase the accuracy of the numerical solution, such as the time-space domain dispersion-relation-based method (Liu and Sen, 2011), the simulated annealing algorithm (Zhang and Yao, 2013), and the least-squares method (Yang et al., 2015). However, a conventional-grid (CG) is ~~also~~ often directly obtained from the second-order wave equation. These methods include the central scheme (Alford et al., 1974; Igel et al., 1995), the high-order compact finite-difference method (Fornberg, 1990), the Lax-Wendroff correction (LWC) scheme (Lax and Wendroff, 1964; Dablain, 1986; Blanch and Robertsson, 2010), the nearly analytical discrete method (Yang et al., 2003), and the nearly analytical central difference method (Yang et al., 2012).

The algorithm design of the CG scheme is easier to use than that of the SG scheme because the variable definition is uniform throughout the grid. However, it is ~~not easy~~hard to determine which of the two schemes is more accurate and efficient. Although the SG scheme has sometimes been regarded as more precise than the CG scheme (Huang and Dong, 2009), there is also some theoretical and experimental proof in the literature that does not support this proposition. Moczo et al. (2011) compared the accuracy of the different finite-difference schemes with respect to the P-wave to S-wave speed ratio using theoretical analysis and numerical experiments. Their investigation ~~determined~~showed that the relative local errors of the CG scheme are almost equal to those of the SG scheme when modeling planar S waves propagating in an unbounded homogeneous elastic isotropic medium with a low P-wave to S-wave ~~speed~~velocity ratio (Vp/Vs=1.42). They ~~determined~~showed that only at higher P-wave to S-wave ~~speed~~velocity ratios (Vp/Vs=5,10) will the relative local error of the CG scheme increase faster than that of the SG scheme, but the difference in the relative local errors of the two schemes will decrease when using a higher-order spatial scheme, i.e., from second-order to fourth-order in space. Moczo et al. (2011) also ~~determined~~showed that the insufficient accuracy of the CG scheme at higher P-wave to S-wave speed ratios can be compensated for by using a higher spatial sampling ratio~~;~~, i.e., a smaller grid size. This

means that a CG scheme with a sufficiently small grid size will be as precise as the SG scheme or better, even if the P-wave to S-wave speed ratio is high. The computational cost of the SG scheme is significantly higher than that of an equal-sized CG scheme, ~~because~~as two variables (velocity and stress) ~~must~~have to be calculated in the SG scheme and only one variable (displacement) ~~must~~have to be computed in the CG scheme.

Reflection from the artificial boundaries introduced by the limited computational area is another numerical source of error~~, which can be eliminated with a wave field modeling algorithm.~~. Over the past thirty years, many techniques have been developed for boundary processing: paraxial conditions (Clayton and Engquist, 1977; Reynolds, 1978; Higdon, 2012), the sponge boundary (Cerjan et al., 1985; Sochacki et al., 1987), the perfectly matched layer (PML) (Berenger, 1994), and the hybrid absorbing boundary conditions (hybrid ABC) (Ren and Liu, 2012). Among these, the PML is one of the most efficient and most commonly used methods. The PML was first introduced for boundary processing of electromagnetic wave equation modeling, after which, it was applied to the elastic-dynamic problem (Chew and Liu, 1996) and acoustic simulations (Liu and Tao, 1998). Many modified versions of the PML, such as the convolutional PML (Komatitsch and Martin, 2007), were subsequently proposed. Gao et al. (2017) compared most of the typical artificial absorbing boundary processing approaches for use with acoustic wave equations and came to the conclusion that a 20-layer PML is ideal for most practical applications using general size models, even in the presence of strong nearly grazing waves, which demonstrates the high performance and efficiency of the PML approach.

In the field of real wave field simulation, most researchers are devoted to unifying the format of the boundary processing algorithm and the wave equation within the computational region. The classic PML is naturally formulated based on the first-order wave equations for velocity and stress (Collino and Tsogka, 1998), which has proven to be very efficient. It is easy to integrate PML boundary processing into a SG finite-difference algorithm. So some scholars use the SG scheme in the computational region to match the PML equations, while for many CG-based schemes, they need to adopt other boundary processing methods, such as the hybrid ABC method. However, in recent years, some scholars have also made efforts to formulate a PML for a second-order system to match the second-order wave equation. Komatitsch and Tromp (2003) reformulated the classic PML conditions in order to use it with numerical schemes that are based on the elastic wave equation written as a second-order system with displacement. Grote and Sim (2010) proposed a PML formulation for the acoustic wave equation in its standard second-order form, while Pasalic and McGarry (2010) extended the convolutional PML to accommodate the second-order acoustic wave equation. Nevertheless, all of these second-order PML formulations require the derivation of ~~complex~~complicated formulas, the introduction of auxiliary variables, and the modification of existing second-order numerical codes in order to handle the first-order equations describing the auxiliary variables, which increases the computational cost and complexity.

In order to preserve the original efficiency of the PML boundary processing method ~~and~~as well as the accuracy and efficiency of the CG scheme, it is worth trying to integrate the classic first-order PML algorithm into the CG finite-difference scheme in a second-order system, and make it easy to implement. In this paper, we propose a new boundary matched algorithm that uses a CG finite-difference scheme within a limited computational area and an SG finite-difference scheme in a PML area. Our approach enables the inner area and the PML condition to be independent during computation, while preserving the individual advantages of the two methods. The algorithm matches the computational area and the absorbing boundary layers simply by point updating along the ~~sides~~boundaries of the computational area and avoids complex formula conversion. Thus,

none of the original formulas of the CG scheme or the PML equations are modified and no unnecessary variables are added. The assessment of the proposed algorithm is composed of two parts. First, we compared the accuracy and efficiency of the proposed algorithm with those of the classic SG PML method (SG scheme both in computational area and PML area), which ~~proved~~demonstrated the rationality of our decision to use the CG scheme in the computational area. To ~~be closer to~~simulate the actual underground medium, a medium with a linearly increasing velocity gradient was selected for the experiment. The experimental results ~~indicate~~indicated that the accuracy of the two methods for equal grid sizes is almost equal, but the efficiency of our method is approximately 30–50 % higher than that of the classic SG PML method. Next, the proposed algorithm was evaluated by comparing its absorption efficiency and computational cost with those of the classic SG PML method, the second-order PML method (CG scheme both in computational area and PML area) introduced by Pasalic and McGarry (2010), and the hybrid ABC method (CG scheme in computational area and hybrid ABC scheme in boundary area) introduced by Ren and Liu (2012). The numerical experimental results ~~indicate~~indicated that our algorithm provides an excellent absorption effect~~, is more efficient,~~ and ~~is~~was easier to implement.

2. Methodology

Although the elastic wave equation can describe the propagation of seismic waves more comprehensively, modeling an elastic wave field is complex and computationally expensive. In practice, the acoustic wave equation is also popularly used to approximate seismic wave propagation. For the convenient error analysis of these methods, we consider a scalar wave field p propagating through an unbounded three-dimensional medium where the wave field satisfies Eq. (1) (Engquist and Runborg, 2003).

$$\frac{\partial^2 p}{\partial x^2} + \frac{\partial^2 p}{\partial y^2} + \frac{\partial^2 p}{\partial z^2} = \frac{1}{c^2} \cdot \frac{\partial^2 p}{\partial t^2}. \tag{1}$$

~~Where~~where the wave field p is a function of the space variables *x, y, z* and the time variable *t*, and *c* is ~~sound~~ velocity of the medium. Numeric modeling of Eq. (1) is expressed as follows.

2.1 Conventional-grid finite-difference scheme

The discretization of the acoustic wave equation (1) with a 2*M*-order finite-difference scheme is (Chu and Stoffa, 2012)

$$p_{i,j,k}^{n+1} = 2p_{i,j,k}^n - p_{i,j,k}^{n-1} + \frac{c^2 \Delta t^2}{\Delta x^2} [c_0 p_{i,j,k}^n + \sum_{m=1}^{M} c_m (p_{i-m,j,k}^n + p_{i+m,j,k}^n)]$$

$$+ \frac{c^2 \Delta t^2}{\Delta y^2} [c_0 p_{i,j,k}^n + \sum_{m=1}^{M} c_m (p_{i,j-m,k}^n + p_{i,j+m,k}^n)]$$

$$+ \frac{c^2 \Delta t^2}{\Delta z^2} [c_0 p_{i,j,k}^n + \sum_{m=1}^{M} c_m (p_{i,j,k-m}^n + p_{i,j,k+m}^n)]. \tag{2}$$

~~Where~~where c_m for all *m* are finite-difference coefficients. *i, j* and *k* denote the discrete spatial variables, and *n* denotes the discrete time variable. The increments Δx, Δy and Δz are grid spacings, and Δt is the time step. In many applications, a regular rectangular grid with a grid spacing $\Delta x = \Delta y = \Delta z = d$ is a natural and reasonable choice (Moczo et al, 2007).

1   Numerical analyses show that grid dispersion increases with increasing grid size, but decreasing the grid

2   size increases the computational cost. High-order finite-difference schemes are able to control this numerical

3   dispersion using a larger grid spacing compared with low-order schemes (Tan and Huang, 2014).

4   Because the subscripts i, j and k used in Eq. (2) have integer values, it is convenient to define and calculate

5   medium's parameters and wave field p for the same grid-points, which leads to the CG scheme. The pressure

6   source s is an additive item (Hustedt et al., 2004), i.e., it can be directly added in the corresponding equations.

7   **2.2 Boundary conditions**

8   Owing to limitations in the capacity and speed of computer facilities, the numerical simulation of a wave

9   field can only be implemented for a limited area. The computational area is surrounded by artificial boundaries,

10   except for the free surface. As described above, the PML boundary condition can effectively absorb the wave

11   field reflections from the artificial boundaries in order to simulate wave field propagation in an open space. In

12   a PML medium, the wave field p is assumed to be decomposed into sub-components. The PML formulation

13   based on the acoustic equations is as follows (Liu and Tao, 1998):

14    $$\frac{\partial v_x}{\partial t} + \alpha_x v_x = -\frac{1}{\rho}\frac{\partial p}{\partial x},$$

15    $$\frac{\partial v_y}{\partial t} + \alpha_y v_y = -\frac{1}{\rho}\frac{\partial p}{\partial y},$$

16    $$\frac{\partial v_z}{\partial t} + \alpha_z v_z = -\frac{1}{\rho}\frac{\partial p}{\partial z},$$

17    $$\frac{\partial p_x}{\partial t} + \alpha_x p_x = -c^2\rho\frac{\partial v_x}{\partial x},$$

18    $$\frac{\partial p_y}{\partial t} + \alpha_y p_y = -c^2\rho\frac{\partial v_y}{\partial y},$$

19    $$\frac{\partial p_z}{\partial t} + \alpha_z p_z = -c^2\rho\frac{\partial v_z}{\partial z},$$

20    $$p = p_x + p_y + p_z.\tag{3}$$

21   ~~Where~~ α_x, α_y, α_z are the attenuation coefficients in the PML medium. In this paper, the attenuation

22   coefficient was set ~~usingthe~~ using the following function (Wang, 2003)

23    $$\alpha_{ij} = B\left[1 - \sin\left(\frac{j\pi}{2P_{ml}}\right)\right], i = x, y, z; j = 0,1,\dots,P_{ml}.\tag{4}$$

24   ~~Where~~ B is the amplitude of attenuation coefficient, i.e., the maximum value of the coefficient, which we set as

25   400 in the numerical experiment; P_{ml} is the thickness of the PML layer.

26   Using the SG finite-difference scheme to discretize (4), the results are as follows

27    $$v_x^{n+\frac{1}{2}}\left(i+\tfrac{1}{2},j,k\right) = v_x^{n-\frac{1}{2}}\left(i+\tfrac{1}{2},j,k\right) - \alpha_x\Delta t v_x^{n-\frac{1}{2}}\left(i+\tfrac{1}{2},j,k\right)$$

28    $$-\frac{\Delta t}{\rho\Delta x}[p_x^n(i+1,j,k) + p_y^n(i+1,j,k) + p_z^n(i+1,j,k) - p_x^n(i,j,k) - p_y^n(i,j,k) - p_z^n(i,j,k)],$$

29    $$v_y^{n+\frac{1}{2}}\left(i,j+\tfrac{1}{2},k\right) = v_y^{n-\frac{1}{2}}\left(i,j+\tfrac{1}{2},k\right) - \alpha_y\Delta t v_y^{n-\frac{1}{2}}\left(i,j+\tfrac{1}{2},k\right)$$

30    $$-\frac{\Delta t}{\rho\Delta y}[p_x^n(i,j+1,k) + p_y^n(i,j+1,k) + p_z^n(i,j+1,k) - p_x^n(i,j,k) - p_y^n(i,j,k) - p_z^n(i,j,k)],$$

31    $$v_z^{n+\frac{1}{2}}\left(i,j,k+\tfrac{1}{2}\right) = v_z^{n-\frac{1}{2}}\left(i,j,k+\tfrac{1}{2}\right) - \alpha_z\Delta t v_z^{n-\frac{1}{2}}\left(i,j,k+\tfrac{1}{2}\right)$$

32    $$-\frac{\Delta t}{\rho\Delta z}[p_x^n(i,j,k+1) + p_y^n(i,j,k+1) + p_z^n(i,j,k+1) - p_x^n(i,j,k) - p_y^n(i,j,k) - p_z^n(i,j,k)],$$

1 $$p_x^{n+1}(i,j,k) = p_x^n(i,j,k) - \alpha_x \Delta t p_x^n(i,j,k) - \frac{c^2 \rho \Delta t}{\Delta x}[v_x^{n+\frac{1}{2}}\left(i+\frac{1}{2},j,k\right) - v_x^{n+\frac{1}{2}}\left(i-\frac{1}{2},j,k\right)].$$

2 $$p_y^{n+1}(i,j,k) = p_y^n(i,j,k) - \alpha_y \Delta t p_y^n(i,j,k) - \frac{c^2 \rho \Delta t}{\Delta y}[v_y^{n+\frac{1}{2}}\left(i,j+\frac{1}{2},k\right) - v_y^{n+\frac{1}{2}}\left(i,j-\frac{1}{2},k\right)].$$

3 $$p_z^{n+1}(i,j,k) = p_z^n(i,j,k) - \alpha_z \Delta t p_z^n(i,j,k) - \frac{c^2 \rho \Delta t}{\Delta z}[v_z^{n+\frac{1}{2}}\left(i,j,k+\frac{1}{2}\right) - v_z^{n+\frac{1}{2}}\left(i,j,k-\frac{1}{2}\right)]. \qquad (5)$$

4 **2.3 Implementation of our new boundary matched algorithm**

5 A finite-difference scheme based on a CG requires no computation of intermediate variables, and thus, the

6 computational cost is lower than that of an SG scheme. We will show in the next section that the accuracy of

7 the CG scheme can reach the same level as that of the SG scheme, but with lower computational costs. However,

8 it is difficult to ~~integrate~~incorporate a naturally formulated,~~available~~ PML boundary processing algorithm

9 based on an SG scheme into a CG finite-difference scheme. In this paper, we propose a new boundary matched

10 algorithm that can ~~seamlessly connect~~bridge the gap between an SG-based PML algorithm ~~to~~and a CG-based

11 numerical simulation of a seismic wave field with neither introduction of intermediary variables nor

12 reformulation of the PML equations. The core idea of the scheme is to interface the wave field reasonably along

13 the boundaries between the CG area and the SG absorbing layers. A detailed description of the method is given

14 below.

15 As shown in Fig. 1, the entire domain consists of two parts: the computational area and the boundary

16 absorbing area. The computational area is located in the center and is surrounded by the absorbing layers. The

17 algorithm uses a CG finite-difference scheme within the computational area and an SG finite-difference scheme

18 within the boundary absorbing area. If we can reasonably interface the computed values of the wave field

19 between the computational area and the boundary absorbing area, then the scheme can perform satisfactorily.

20 For a clearer explanation, we start with a two-dimensional model.

21 We let the computational area and the PML area overlap each other for one layer. As shown in Fig. 1(a),

22 the bold red boundary line is both the outermost ~~layer~~boundary of the computational area and the innermost

23 ~~layer~~boundary of the PML area. On this overlapped layer, both the particle velocity v and the wave field p in

24 the PML area are calculated using the value of wave field p in the computational area. Using this method, the

25 two areas can be connected. This avoids the introduction of intermediate variables and saves storage space. In

26 order to distinguish, we use $p_{i,j}^{n+1}$ to represent the wave field value in the computational area, and $p_x^n(i,j)$ and

27 $p_z^n(i,j)$ to represent the wave field value in the PML area. In the PML area, the values of attenuation

28 coefficients α_x and α_z can be calculated using Eq. (4). When the grid points are located on the four corners of

29 the PML area, the values of α_x and α_z are not zero. When they are on the left- and right-hand sides of the

30 PML area, $\alpha_x \neq 0$ and $\alpha_z = 0$; when they are on the upper and ~~lower~~bottom sides of the PML area, $\alpha_x = 0$

31 and $\alpha_z \neq 0$. The specific steps of our method are as follows.

a)

b)
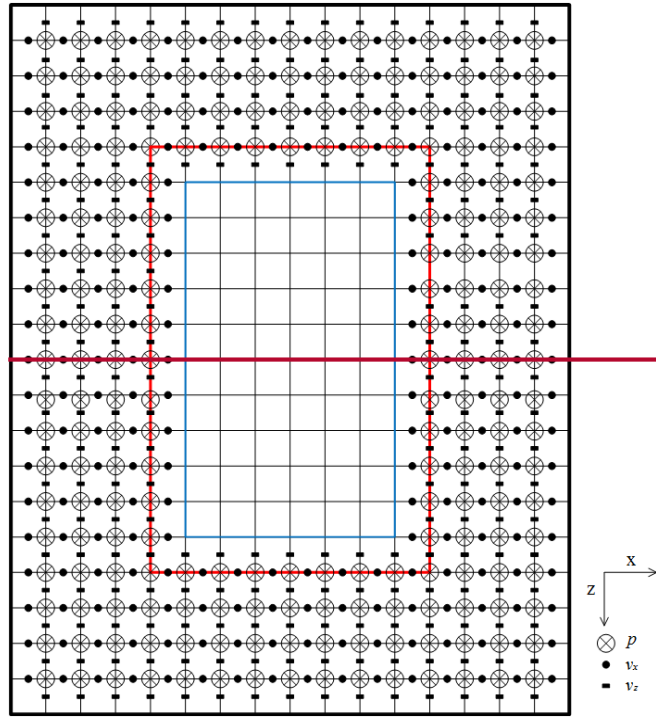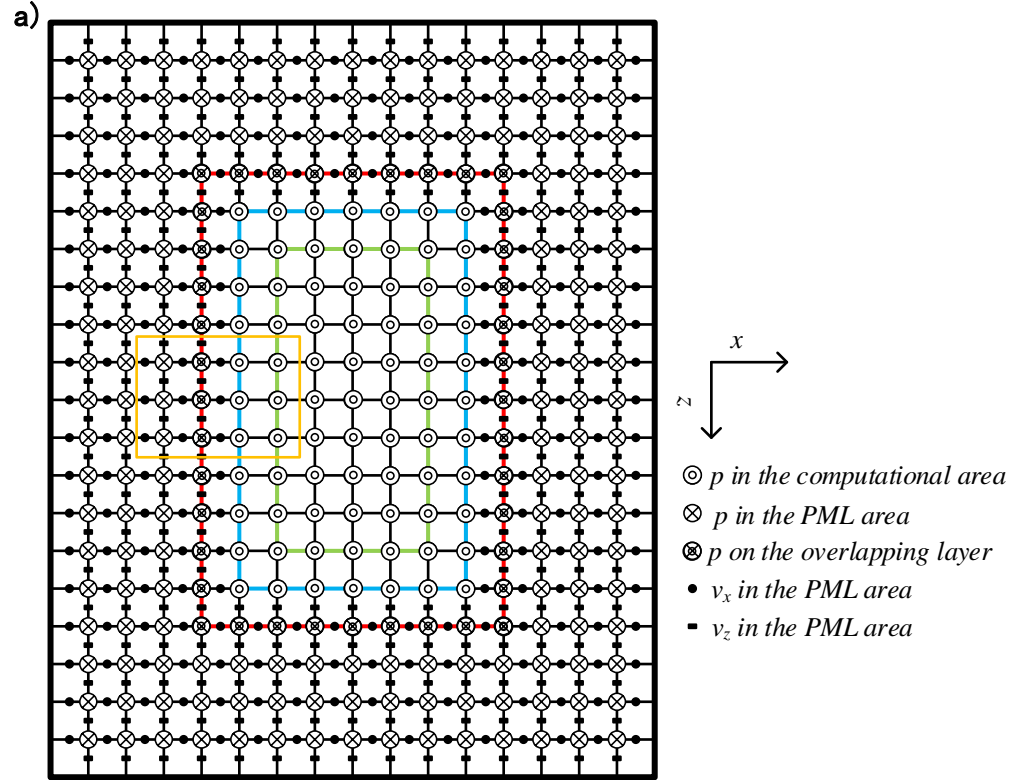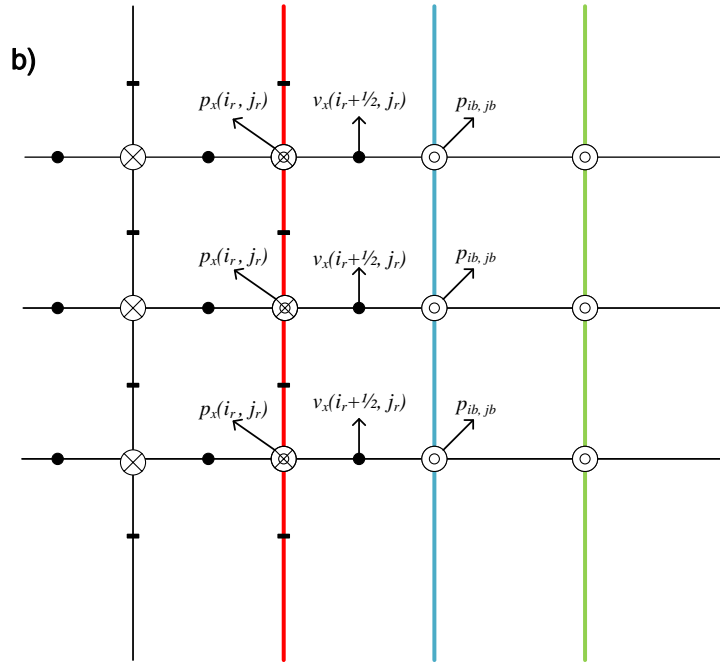
Figure 1. Schematic of our method: (a) the entire region~; (b) partial enlargement of the yellow rectangle~ in (a).

1. At the beginning of iteration, take n = 1, let the initial wave field values $p_{i,j}^n$ and $p_{i,j}^{n-1}$ in the computational area, the particle velocity $v_x^{n-\frac{1}{2}}\left(i+\frac{1}{2},j\right)$ and $v_z^{n-\frac{1}{2}}\left(i,j+\frac{1}{2}\right)$, the wave field $p_x^n(i,j)$ and $p_z^n(i,j)$ in the PML area all be zero.

2. Calculate the wave field $p_{i,j}^{n+1}$ in the computational area. In this step, we do not calculate the value of wave field $p_{i,j}^{n+1}$ located on the red boundary line; ~that is~instead, we only calculate them on the blue boundary

line and in its inner region in Fig. 1 using the two-dimensional form of Eq. (2). For the high-order difference scheme in the computational area, we use the second-order difference scheme for the grid points on the blue rectangular line, the fourth-order difference scheme for the grid points on the inner green rectangular line, and the sixth-order difference scheme on the inner layer, and so on, until we reach the required order of difference. In this way, the computational area and the PML area can be independent, and the number of overlapping layers does not increase with the increase of order of difference. The numerical experiments in section 4.1 will prove that our treatment to the boundary does not bring much additional dispersion and error.

3. Calculate the particle velocity and wave field in the PML area layer by layer, ~~from left to right and from top to bottom~~. Calculate the values of all particle velocity $v_x^{n+\frac{1}{2}}\left(i+\frac{1}{2},j\right)$ and $v_z^{n+\frac{1}{2}}\left(i,j+\frac{1}{2}\right)$ in the PML area (including those on the red line) using the two-dimensional forms of the first and ~~second~~third formulas in Eq. (5). Calculate the all of the wave field values $p_x^{n+1}(i,j)$ and $p_z^{n+1}(i,j)$ in the PML area (including those on the red line) using the two-dimensional forms of the fourth and ~~fifth~~sixth formulas in Eq. (5).

It is important to note that the particle velocities in the area between the blue and red lines is calculated from the wave field $p_x^n(i_r,j_r)$ and $p_z^n(i_r,j_r)$ on the red line in the PML area and the wave field p_{i_b,j_b}^n on the blue line in the computational area. ~~Using Eq. (6~~As shown in Fig. 1(b), we can obtain $v_x^{n+\frac{1}{2}}\left(i_r+\frac{1}{2},j_r\right)$ for the line between the left-hand line of the red rectangle and blue rectangle; ~~Using~~ using Eq. (6), the subscript r stands for the grid points on the red lines, and b stands for the blue lines. Similarly, we can obtain $v_x^{n+\frac{1}{2}}\left(i_r-\frac{1}{2},j_r\right)$ between the ~~left of~~right-hand line of two rectangles; using Eq. (7); for the line between the upper lines, we obtain $v_z^{n+\frac{1}{2}}\left(i_r,j_r+\frac{1}{2}\right)$ using Eq. (8); for the line between the lower lines, we obtain $v_z^{n+\frac{1}{2}}\left(i_r,j_r-\frac{1}{2}\right)$ using Eq. (9):

$$v_x^{n+\frac{1}{2}}\left(i_r+\frac{1}{2},j_r\right) = v_x^{n-\frac{1}{2}}\left(i_r+\frac{1}{2},j_r\right) - \alpha_x\Delta t v_x^{n-\frac{1}{2}}\left(i_r+\frac{1}{2},j_r\right) - \frac{\Delta t}{\rho\Delta x}[p_{i_b,j_b}^n - p_x^n(i_r,j_r) - p_z^n(i_r,j_r)]. \ (6)$$

$$v_x^{n+\frac{1}{2}}\left(i_r-\frac{1}{2},j_r\right) = v_x^{n-\frac{1}{2}}\left(i_r-\frac{1}{2},j_r\right) - \alpha_x\Delta t v_x^{n-\frac{1}{2}}\left(i_r-\frac{1}{2},j_r\right) - \frac{\Delta t}{\rho\Delta x}[p_x^n(i_r,j_r) + p_z^n(i_r,j_r)-p_{i_b,j_b}^n]. \ (7)$$

$$v_z^{n+\frac{1}{2}}\left(i_r,j_r+\frac{1}{2}\right) = v_z^{n-\frac{1}{2}}\left(i_r,j_r+\frac{1}{2}\right) - \alpha_z\Delta t v_z^{n-\frac{1}{2}}\left(i_r,j_r+\frac{1}{2}\right) - \frac{\Delta t}{\rho\Delta z}[p_{i_b,j_b}^n - p_x^n(i_r,j_r) - p_z^n(i_r,j_r)]. \ (8)$$

$$v_z^{n+\frac{1}{2}}\left(i_r,j_r-\frac{1}{2}\right) = v_z^{n-\frac{1}{2}}\left(i_r,j_r-\frac{1}{2}\right) - \alpha_z\Delta t v_z^{n-\frac{1}{2}}\left(i_r,j_r-\frac{1}{2}\right) - \frac{\Delta t}{\rho\Delta z}[p_x^n(i_r,j_r) + p_z^n(i_r,j_r)-p_{i_b,j_b}^n]. \ (9)$$

After calculating the complete PML area, let the value of the wave field $p_{i,j}^{n+1}$ on the red line in the computational area be equal to the sum of the wave field $p_x^{n+1}(i_r,j_r)$ and $p_z^{n+1}(i_r,j_r)$ on the red line in the PML area.

4. Update the value of $p_{i,j}^{n-1}$ with the value of $p_{i,j}^n$, and update the value of $p_{i,j}^n$ with the value of $p_{i,j}^{n+1}$; then, let $n = n + 1$.

5. Repeat steps 2–4 until n reaches the required time length.

The two-dimensional algorithm described above can easily be generalized to three-dimensional. In the three-dimensional model, we need to add a particle velocity component v_y and a space position label k. The red and blue boundary lines become the red and blue boundary surfaces, respectively. In addition, the computational area becomes a cube surrounded by the PML area.

1 **3. Performance analysis**

2 As described in the Introduction, the errors in the wave field numerical model are mainly caused by

3 differential dispersion and reflected waves that are not fully absorbed by the boundary processing algorithm. In

4 order to verify the validity of our algorithm, we used a variety of models to compare the computational accuracy,

5 the efficiency of the absorption of the reflected waves, and the computational efficiency of the proposed

6 algorithm to the other methods.

7 **3.1 Computational accuracy ~~formula~~**

8 In order to obtain a more convincing result when comparing the computational accuracy, we used a

9 constant-gradient velocity model, the velocity of which increases linearly with depth. This model is closer to

10 the actual velocity distribution of an underground medium than a homogeneous model. We calculated the

11 relative error between our method and the classic SG PML method using the analytical solutions for different

12 grid spacings and the order of difference, and then, we performed a comparative analysis of the two methods.

13 The relative error between the two methods and the analytical solution is defined by the following time function:

14 $$\text{error(t)} = 20\log\left|\frac{p(t)-p_{anal}(t)}{\max[p_{anal}(t)]}\right|. \qquad (10)$$

15 ~~Where~~In equation (10), $p(t)$ represents the value of wave field calculated by the numerical methods at a

16 receiving point, and $p_{anal}(t)$ is the value of wave field calculated by ~~theanalytic~~the analytic solution at the

17 same receiving point.

18 For the two-dimensional scalar equation (1), the wave field analytic solution for a ~~homogeneous~~constant-

19 gradient medium can be obtained from the integral form of the three-dimensional solution using the dimension

20 reduction method (Cerveny, 2001). The velocity distribution is $c(z) = c(z_0)\frac{1+\gamma z}{1+\gamma z_0} = c(0)(1 + \gamma z)$, where z_0

21 is the depth of source, $c(z_0)$ is the velocity of the source layer, $c(0)$ is the velocity of the layer $z = 0$, and

22 $\gamma = \frac{1}{h}$, ~~where $c(-h) = 0$.~~h is the distance from depth $z = 0$ to the level where the propagation velocity is null

23 $(c(-h) = 0)$. When the line source $s = \delta(t - t_0)\delta(x - x_0)\delta(z - z_0)$ is located at (x_0, z_0), and the density in

24 the method of Sanchez-Sesma et al. (2001) is a constant, a two-dimensional scalar Green's function can be

25 obtained by

26 $$G(x, z, t) \approx \Lambda \cdot \frac{H(t-t_0-\tau)}{2\pi\sqrt{(t-t_0)^2-\tau^2}}. \qquad (11)$$

27 ~~Where~~where $\Lambda = \sqrt{\frac{1+\gamma z_0}{1+\gamma z} \cdot \frac{c(z_0)\tau}{R_w}}$.

28 $H(t)$ is the Heaviside step function (equal to 0 when t<0 and equal to 1 when t>0)~~.~~ For fixed t, the radius

29 R_w of the wavefront circle is $R_w = (z_0 + h)\sinh(\gamma c(0)\tau)$ and the traveltime τ can be computed by means

30 (Cerveny, 2001) of $\tau = \left|\frac{1}{\gamma c(0)}~~arecosh~~arccosh[1 + \frac{(\gamma c(0)r)^2}{2c(z)c(z_0)}]\right|$, $r = \sqrt{(x - x_0)^2 + (z - z_0)^2}$. This is an

31 approximate solution, but usually the error is less than 1% (Sanchez-Sesma et al., 2001). In the next numerical

32 experiment, we use a symmetric Ricker wavelet with a peak frequency of 20 Hz as the source. In this paper, the

33 expression is usually $s(t) = \{1 - 2[20\pi(t - t_0 - 1/20)]^2\}e^{-[20\pi(t-t_0-1/20)]^2}$~~,~~ and t_0 is equal to 200 ms. The

34 final result of the analytic solution is

35 $$p_{anal}(x, z, t) = G(x, z, t) * \delta(x - x_0)\delta(z - z_0)S(t) \qquad (12)$$

1 **3.2 Absorption efficiency ~~formula~~ of the reflected waves**

2   When comparing the absorption efficiency, we used three different geological models to determine the

3 reflected wave absorption effect of our algorithm: the homogeneous, constant-gradient velocity and the

4 Marmousi models. We compared the absorption effects of our algorithm with the classic SG PML method, the

5 second-order PML method, and the hybrid ABC method using the same conditions to prove whether our

6 algorithm can effectively combine the CG scheme with the SG scheme PML boundary condition and achieve

7 the same or better effect as other methods do. In the computational area, the reflection coefficient R of a

8 receiving point is defined as

9     $R = 20\log|\frac{\max[p(t)-p_{ref}(t)]}{\max[p_{ref}(t)]}|$ (13)

10 Where the wave field value $p(t)$ is calculated by the numerical methods at a receiving point, and $p_{ref}(t)$ is

11 the wave field value that has no boundary reflection on the same receiving point calculated using the numerical

12 methods, which can be obtained by expanding the model. The value of R reflects the reflected wave absorption

13 effect of the algorithm. The smaller the R value, the better the absorption effect.

14 **3.3 Computational efficiency index**

15   In the comparison of the computational accuracy and efficiency of the absorption of the reflected waves,

16 we determined the computation time of the three methods separately, which can reflect the advantages and

17 disadvantages of all of the methods in terms of the computational efficiency.

18 **4. Numerical experiment**

19   Based on the discussion of the performance analysis, in this section, we present the results of the numerical

20 experiments. All of the numerical experiments were run on a desktop personal computer with a 3.40 GHz Intel

21 Core i5-3570 processor, 32 G of DDR3 memory, on a 64-bit Windows 7 operating system, using algorithmic

22 software written in C ++.

23 **4.1 Computational accuracy and computation time**

24   As shown in Fig. 2, the constant-gradient velocity model has a size of 6000 m×6000 m, a velocity

25 distribution of $c = 500$ m/s for $z = 0$ m and $c = 5300$ m/s for $z = 6000$ m, and a velocity gradient of 0.8. In order

26 to determine the stability of the differential form throughout the computational process, the time step was set

27 as 0.001 s and the total simulation time as 10 s. The sources are located in the middle of the model (3000 m,

28 3000 m), and the three receiving points are located at (600 m, 1800 m), (1800 m, 1800 m), and (3000 m, 1800

29 m). We compared the errors of the numerical solution and the analytical solution at the receiving points of the

30 method we proposed with the classic SG PML methods. The number of PMLs is set as 10. Figure 3 and 4 show

31 the comparison of the analytical solutions at the three receiving points of the proposed method (second-order

32 CG scheme in the computational area) and the classic SG PML method (second-order SG scheme in the

33 computational area) when the grid spacing (d) is ~~12~~12m and ~~10~~10m, respectively. Figure 5 shows the relative

1   errors between the analytical solutions and the two methods for the conditions described above where the

2   relative error was calculated using Eq. (10)
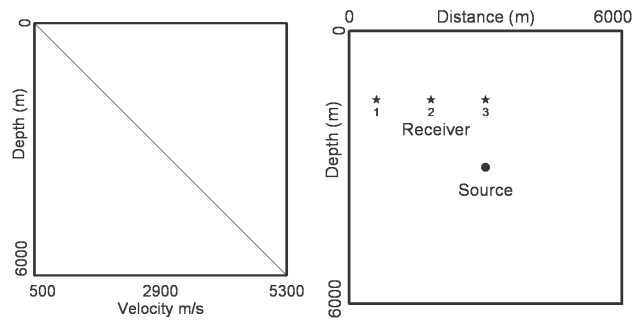
4   **Figure 2.** Velocity profiles in depth and the distribution of source and receiving points.
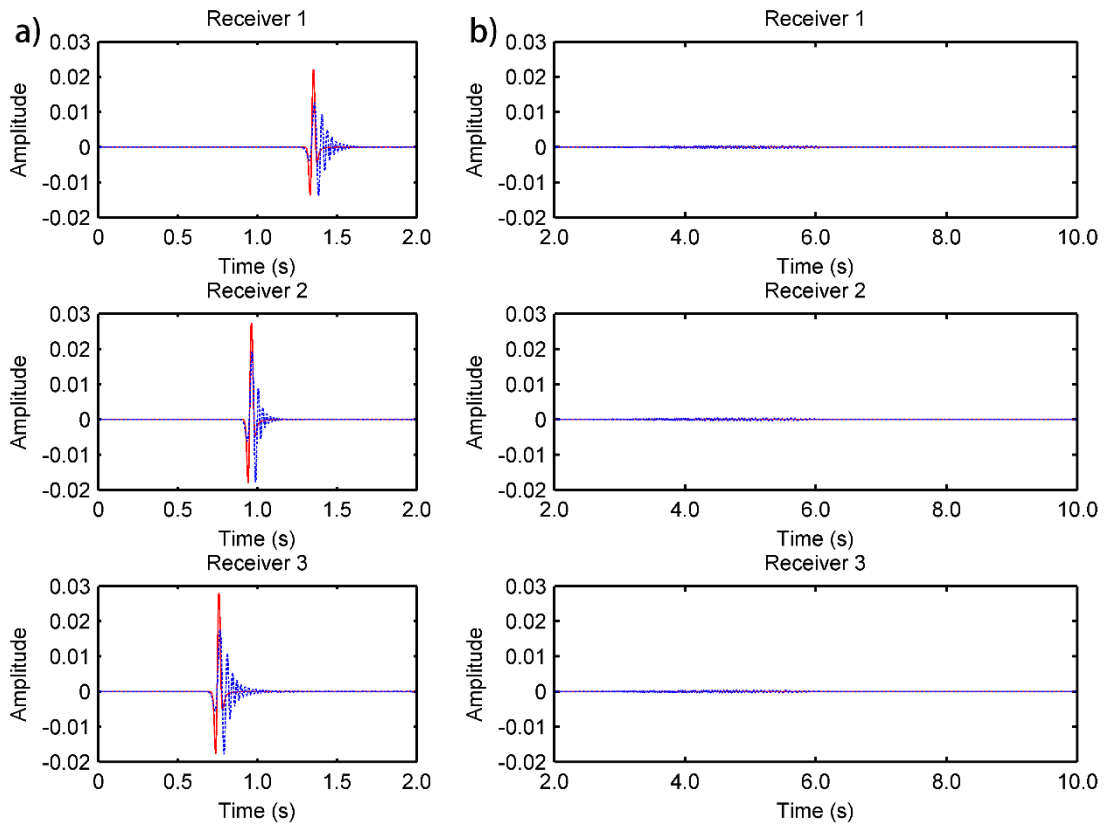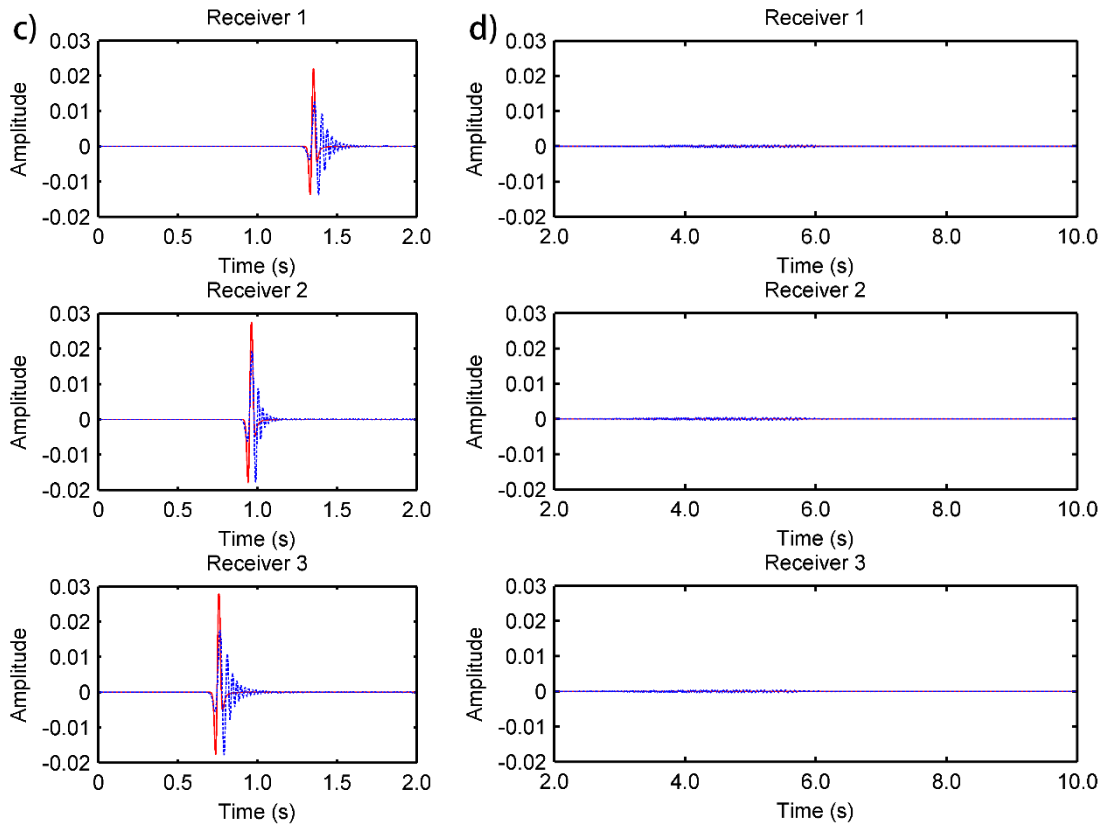
Figure 3. Comparison of the analytical solution (red solid line) with the proposed (second-order CG scheme) and classic SG PML methods (second-order SG scheme) (blue dotted line) at different receiving points, d = 12 m. (a) Proposed method at receivers 1, 2, and 3 for the first two seconds; (b) proposed method at receivers 1, 2, and 3 after two seconds; (c) classic SG PML method at receivers 1, 2, and 3 for the first two seconds; and (d) classic SG PML method at receivers 1, 2, and 3 after two seconds.
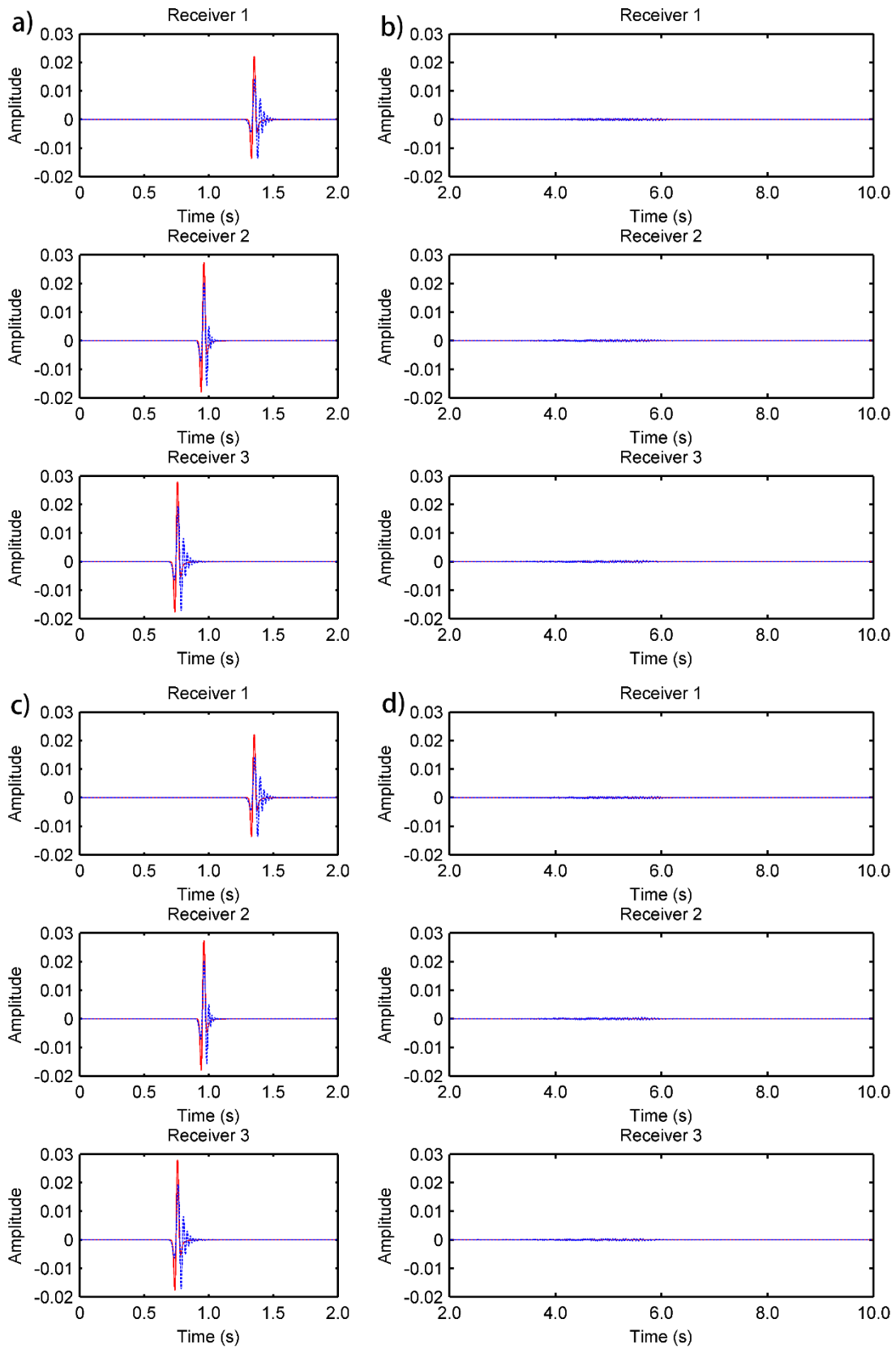
Figure 4. $d = 10$ m; the rest is the same as in Fig. 3.
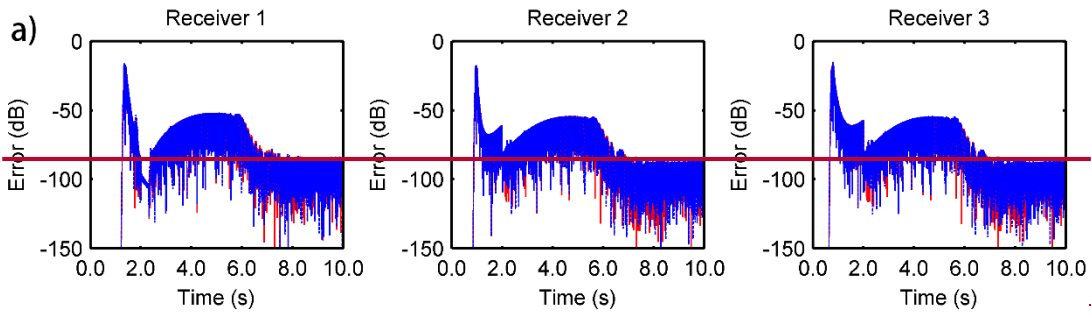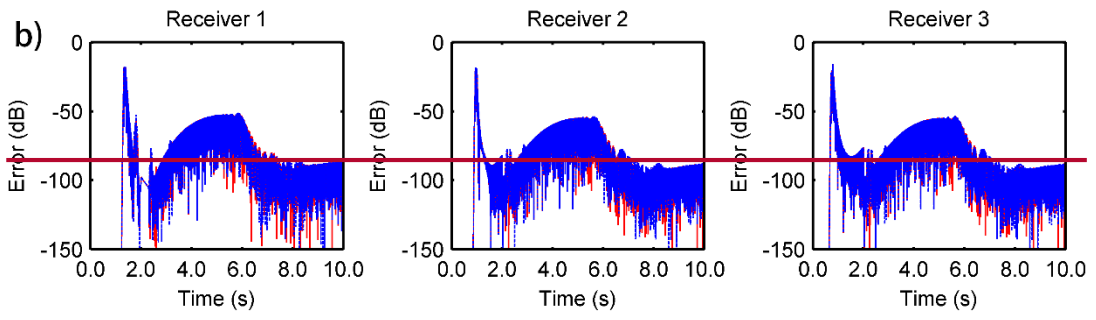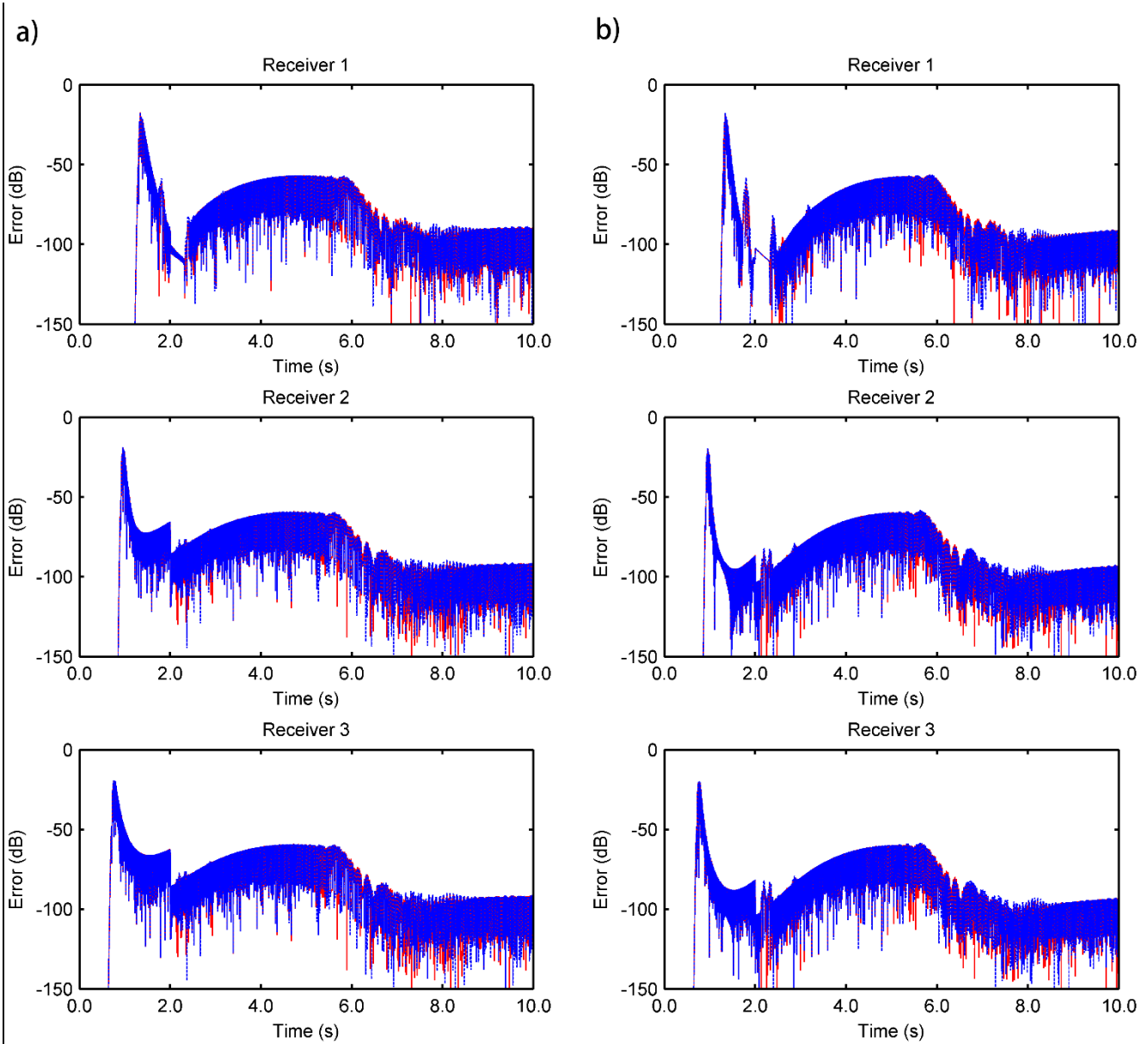
Figure 5. Comparison of the relative errors between the analytical solutions and the proposed method (second-order CG scheme) (red solid line) or the classic SG PML method (second-order SG scheme) (blue dotted line) at different receiving points and different grid spacings. (a) $d = 12$ m, receiving points 1, 2, and 3; (b) $d = 10$ m, receiving points 1, 2, and 3.

From Fig. 3 and 4, we can see that both of the methods have obvious errors during the first two seconds. In particular, when the grid spacing is 12 m, the error is the largest, and there is significant numerical dispersion. Reducing the grid spacing can reduce the error and the dispersion. When the grid spacing is 10 m, the result improves. In addition, the results for a longer simulation time also prove the numerical stability of our method. Further comparison of the relative error curves shown in Fig. 5 indicates that although neither method is particularly good, the ~~amplitude of~~ relative errors ~~of~~with their analytical solutions are almost the same.

In theory, the error of the numerical solution can be reduced by using a higher-order difference. We compared the experimental results of the proposed method (fourth-order CG scheme in the computational area)

1   and classic SG PML methods (fourth-order SG scheme in the computational area) with the analytic solution, as

2   shown in Fig. 6-8.
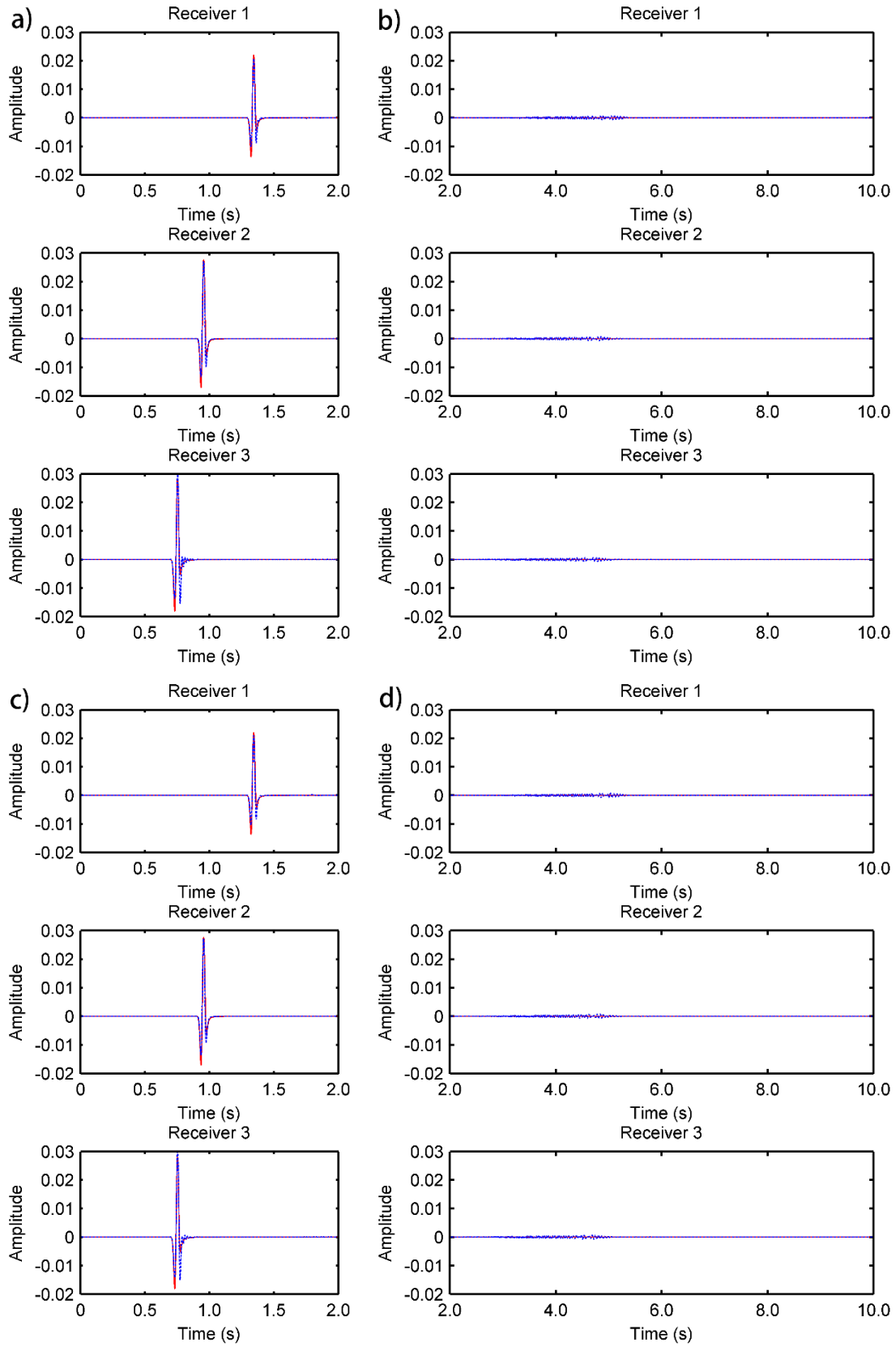
5   **Figure 6.** Comparison of the analytical solution (red solid line) with the proposed (fourth-order CG scheme)

6   and classic SG PML methods (fourth-order SG scheme) (blue dotted line) at different receiving points and $d = 12$

1   m. (a) Proposed method at receivers 1, 2, and 3 during the first two seconds; (b) proposed method at receivers 1, 2,

2   and 3 after two seconds; (c) classic SG PML method at receivers 1, 2, and 3 during the first two seconds; and (d)

3   classic SG PML method at receivers 1, 2, and 3 after two seconds.
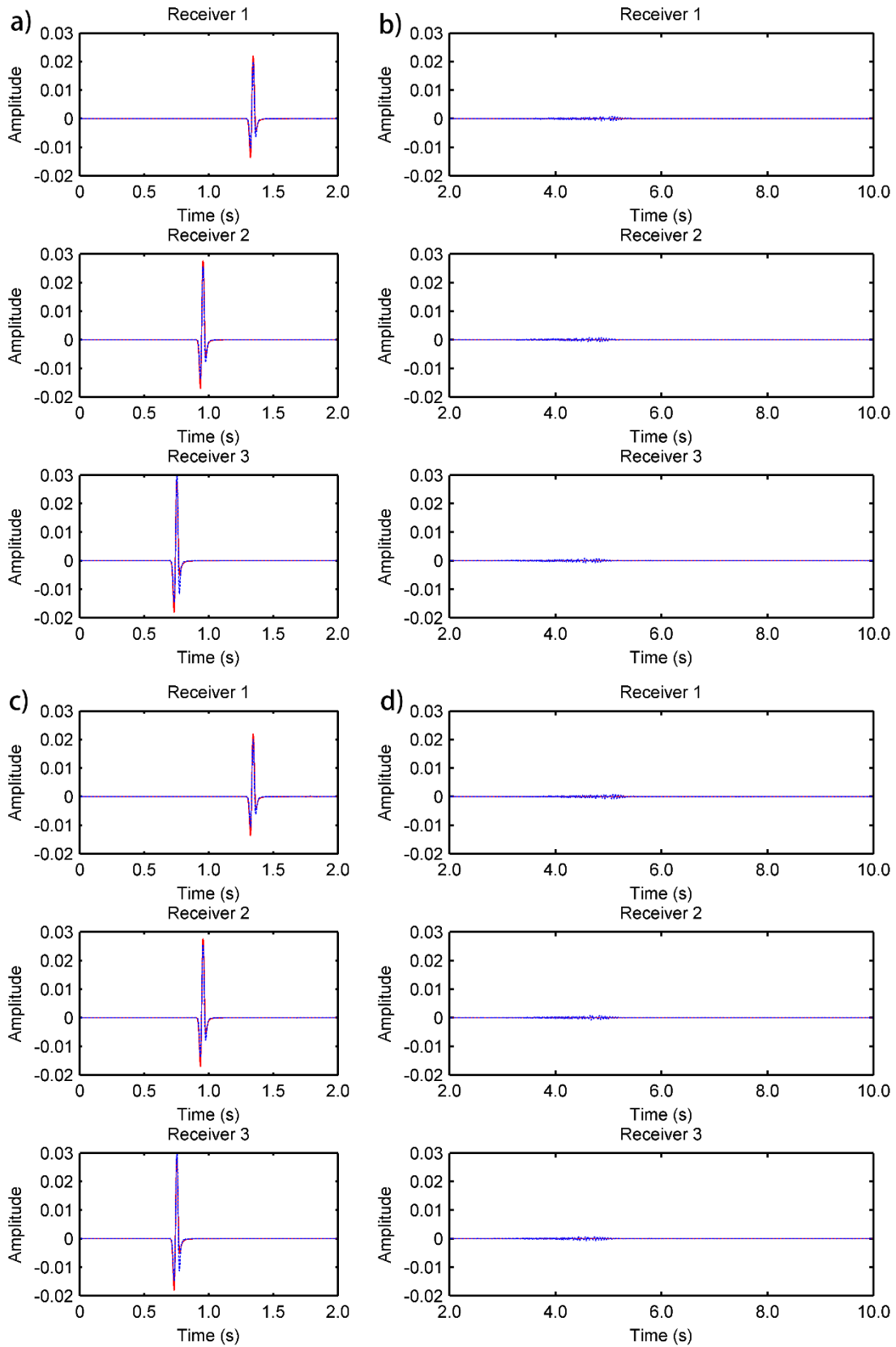
6   **Figure 7.** $d = 10$ m; the rest is the same as in Fig. 6.
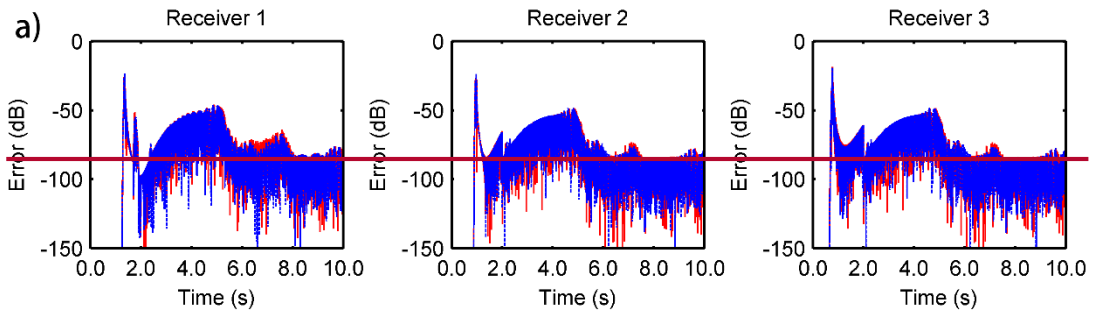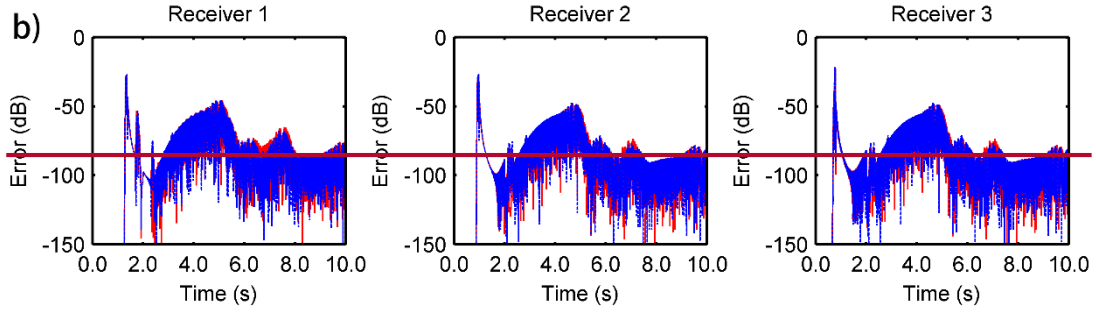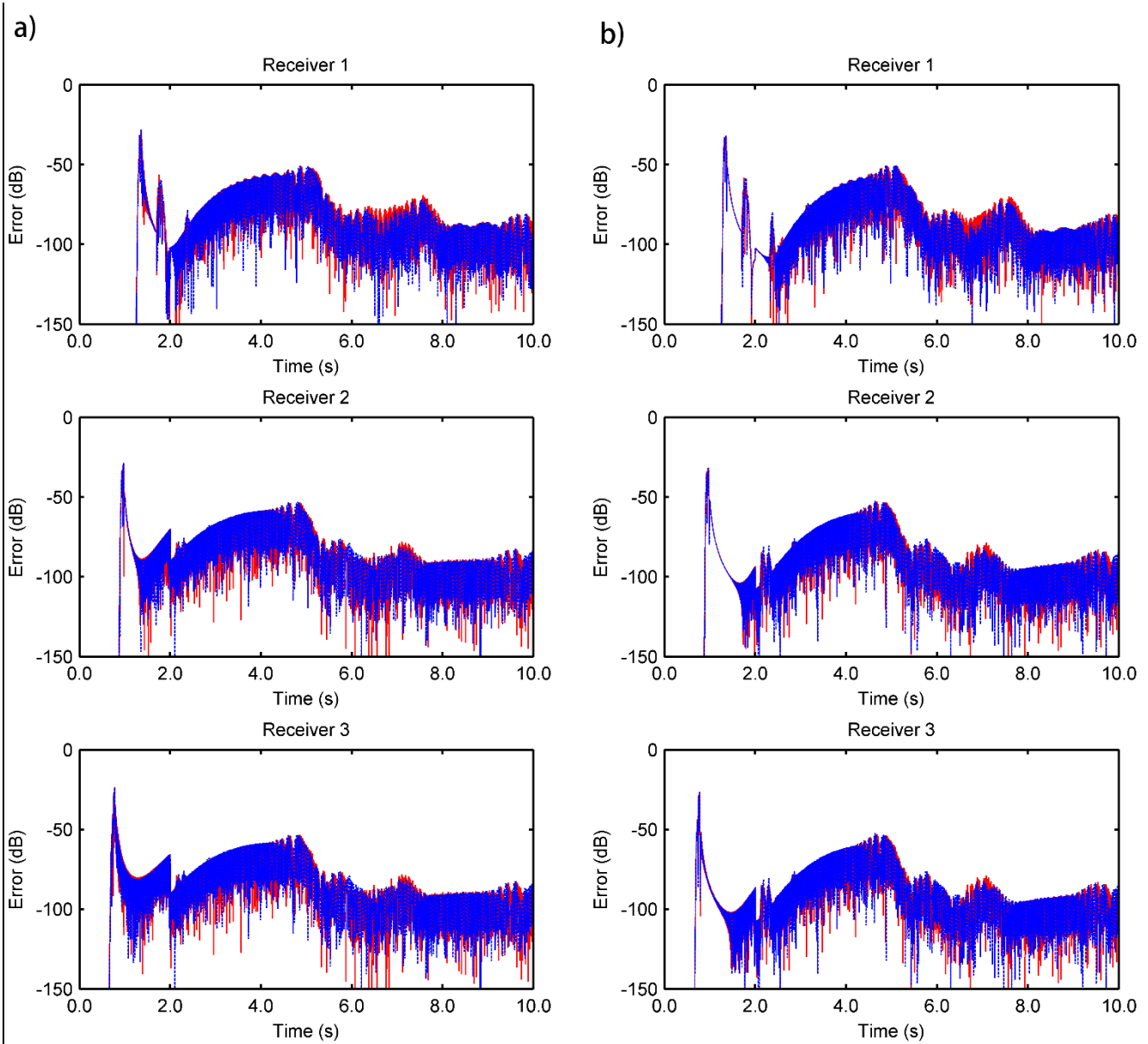
Figure 8. Comparison of the relative errors between the analytical solutions and the proposed method (fourth-order CG scheme) (red solid line) or the classic SG PML method (fourth-order SG scheme) (blue dotted line) at different receiving points and different grid spacings. (a) $d = 12$ m, receiving points 1, 2, and 3; (b) $d = 10$ m, receiving points 1, 2, and 3.

From Fig. 6 and 7, we can see that when the fourth-order difference is used, the relative errors between the analytical solution and both methods are significantly reduced compared with when the second-order difference is used. In addition, as with the second-order result above, the relative error also decreases as the grid spacing decreases. Figure 8 illustrates the fact that the relative error curves of our algorithm and the classic SG PML method are also very similar for the fourth-order difference, In addition, it is difficult to distinguish the advantages and disadvantages of the two algorithms. Although the results of the two methods still exhibit a small error at this time, we can continue to ~~improve~~use higher the difference order or we can reduce the grid spacing to reduce the error~~, but the~~. The laws of the two methods are the same.
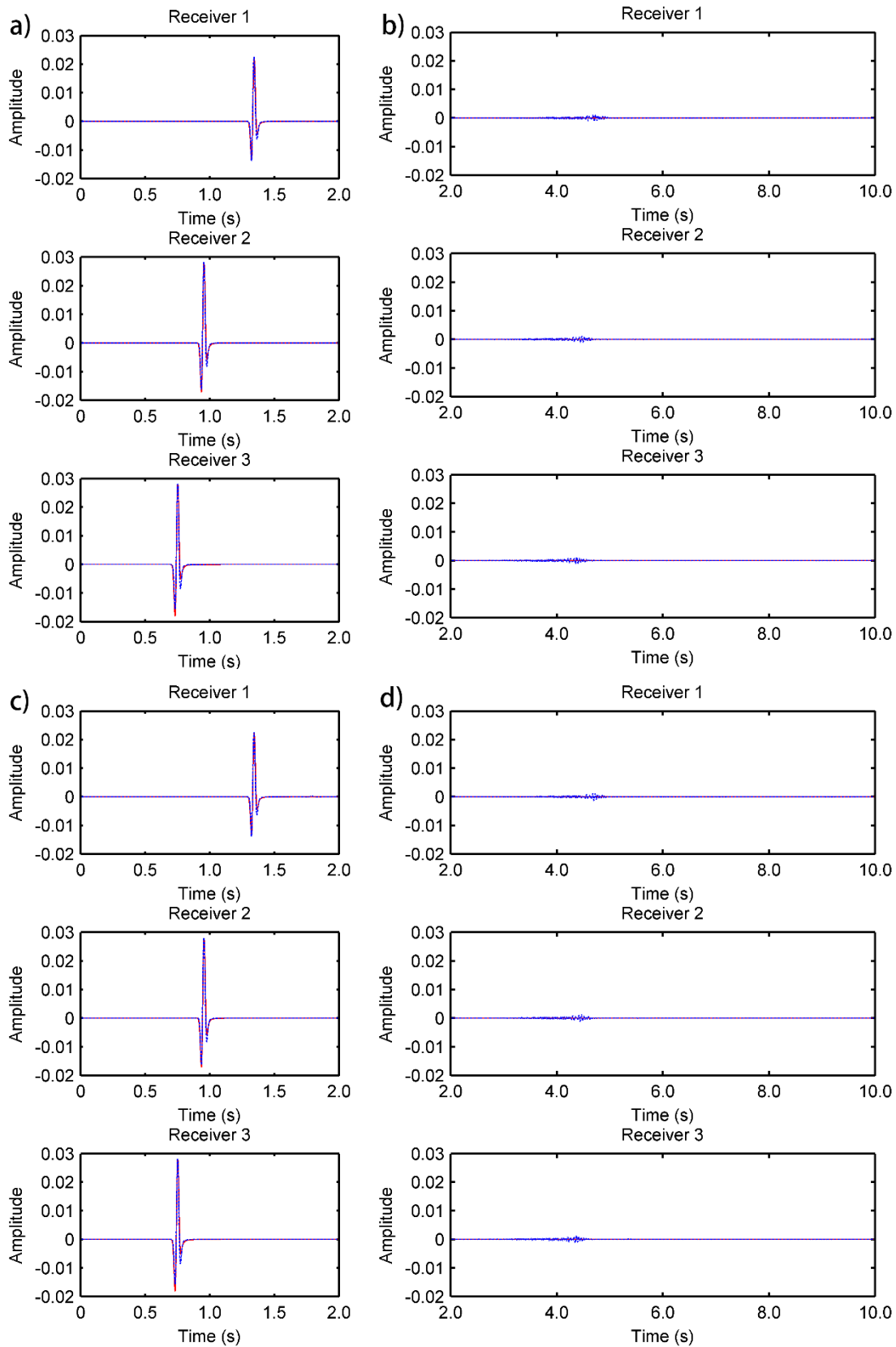
Figure 9 Comparison of the analytical solutions of the proposed (tenth-order CG scheme) (red solid line) and the classic SG PML methods (tenth-order SG scheme) (blue dotted line) at different receiving points, $d =$ 10 m. (a) Proposed method at receivers 1, 2, and 3 during the first two seconds; (b) proposed method at receivers

1, 2, and 3 after two seconds; (c) classic SG PML method at receivers 1, 2, and 3 during the first two seconds;

and (d) classic SG PML method at receivers 1, 2, and 3 after two seconds.
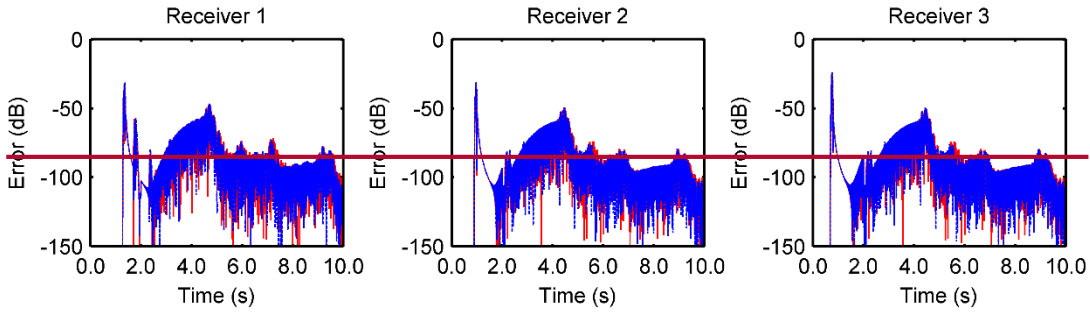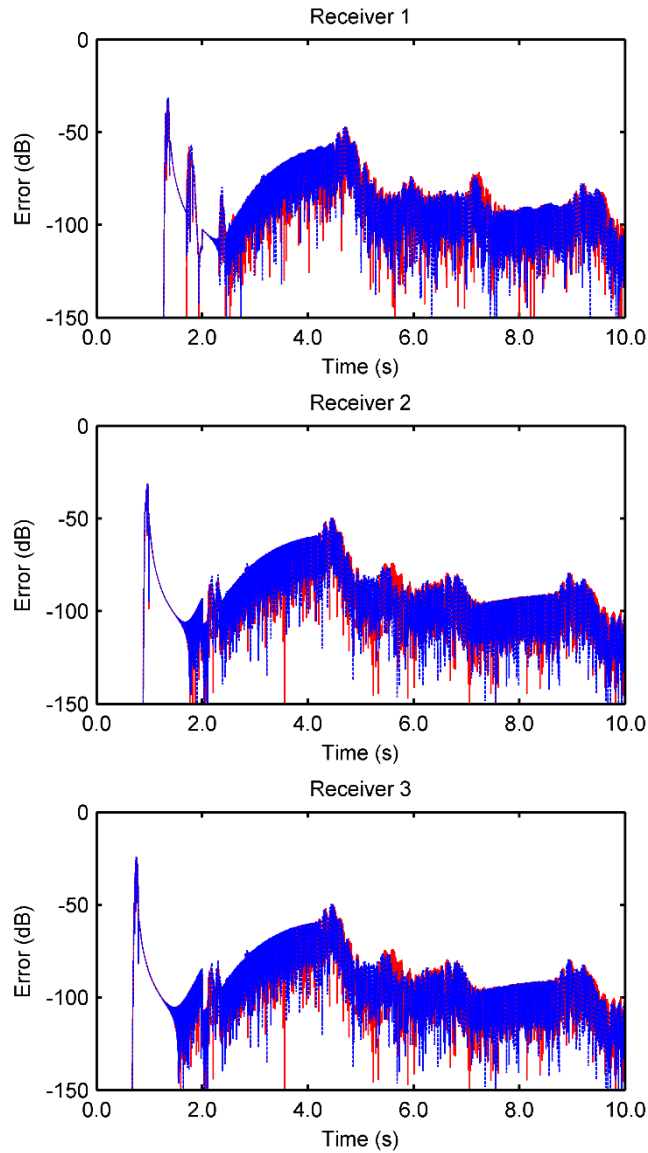
Figure 10. Comparison of the relative errors between the analytical solutions and the proposed method (tenth-order CG scheme) (red solid line) or the classic SG PML method (tenth-order SG scheme) (blue dotted line) at different receiving points and different grid spacings. $d = 10$ m, receiving points 1, 2, and 3.

In Fig. 9 and 10, we adopt a tenth-order difference scheme and $d = 10$ m. At this time, the numerical results are very close to the analytical solution and the relative error is very low. Based on this, we can conclude that the accuracies of the proposed method and the classic SG PML method for the same conditions with a constant-gradient velocity are similar. Meanwhile, it also demonstrates an additional advantage of our method. When the computational area and the PML area are independent of each other, we can easily optimize the numerical algorithm of the computational area to improve the accuracy of the algorithm. When the grid spacing and the order of difference are appropriate, our method yields the expected results. Because our method uses the CG scheme in the computational area, the experimental results also show that in the scalar wave field simulation, the accuracy of the SG scheme is not higher than that of the CG scheme. This conclusion is in agreement with the experimental results of the elastic wave field simulated by Moczo *et al.* (2011) at a low P-wave to S-wave speed ratio ($V_p/V_s=1.42$).

Table 1 presents the computation times of the two methods at different grid spacings and difference orders. The efficiency percentage is the total computation time of our method divided by the total computation time of the SG method. Under the same circumstances, t~~T~~he total computation time of our method is only 57–70 % that of the classic SG PML method. It is noteworthy that the result of our method for the tenth-order difference and a grid spacing of 10 m is much better than that of the classic SG PML method for the fourth-order difference and a 10 m grid spacing, while the computation time is nearly the same. Also, the result of our method for the fourth-order difference and a grid spacing of 12 m is much better than that of the classic SG PML method for the second-order difference and a 10 m grid spacing, while the former computation time is only 53.3 % of the latter. Therefore, for the same computation time as the classic SG PML method, our method always achieves a higher accuracy for a smaller grid spacing and a higher-order difference. We obtained these conclusions in a constant-gradient velocity medium. ~~Of course, these conclusions also apply to other inhomogeneous mediums.~~ Therefore, the algorithm we propose works well when the CG scheme is used in the computational area. Next, we discuss the absorption efficiency of the reflected waves of our method in a series of simple and complex models.

Table 1. Computation time for our and the classic SG PML methods.

condition	Our method	The classic SG PML method	Efficiency percentage
Second-order d=12m	10m 19sec	15m 17sec	67.5%
Second-order d=10m	14m 41sec	21m 01sec	69.8%
fourth-order d=12m	11m 13sec	17m 56sec	62.5%
fourth-order d=10m	16m 58sec	25m 54sec	64.3%
~~tenth-order~~ ~~d=12m~~	~~18m 20sec~~	~~31m 20sec~~	~~58.5%~~
tenth-order d=10m	25m 48sec	44m 54sec	57.4%

1 **4.2 Absorption efficiency and computation time**

2 4.2.1 Homogeneous model

3   First, we used a two-dimensional homogeneous model to verify the reflected wave absorption efficiency

4 of our new boundary matched algorithm. As shown in Fig. 11, the model size is 2000 m×2000 m at a velocity

5 of c = 2500 m/s, and a grid spacing of 10 m. The source is the same as previously described and is located at

6 (1000 m, 1000 m) with a time step of 0.001 s and a total simulation time of 1.5 s. Two hundred and one receiving

7 points are evenly distributed on a horizontal line with a depth of 500 m, and the distance between each receiving

8 point is set as 10 m. In Fig. 12, we compared the receiving point records of our method, the classic SG PML

9 method, the second-order PML method, and the hybrid ABC method for a different number of absorbing layers-.

10 In general, the amplitude of the reflected wave will be reduced to less than 1% of that of the normal wave field

11 after the boundary conditions are processed. Thus, in order to illustrate the reflected wave more clearly, we set

12 the range of the color bar of the wave field to be −0.001 to 0.001. For further comparison, we also calculated

13 the value of the reflection coefficient R using Eq. (13) and plotted the corresponding curve in Fig. 13.
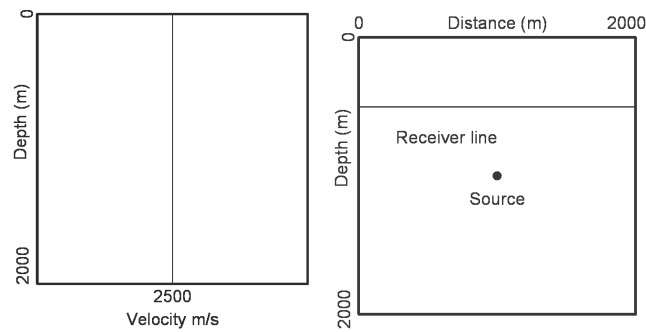
15   **Figure 11.** Velocity profiles with depth and the location of source and receiving points.
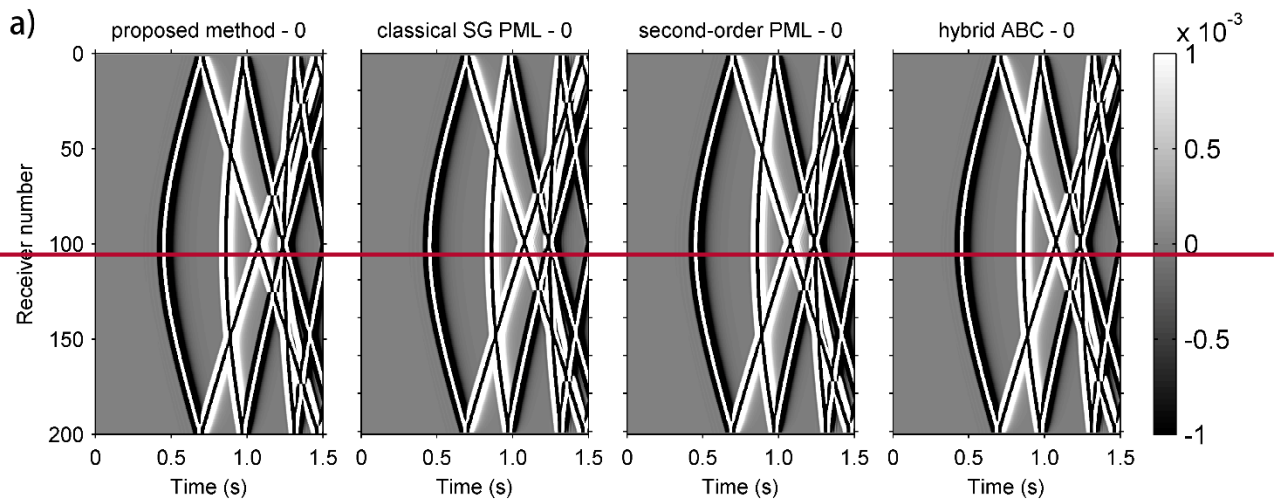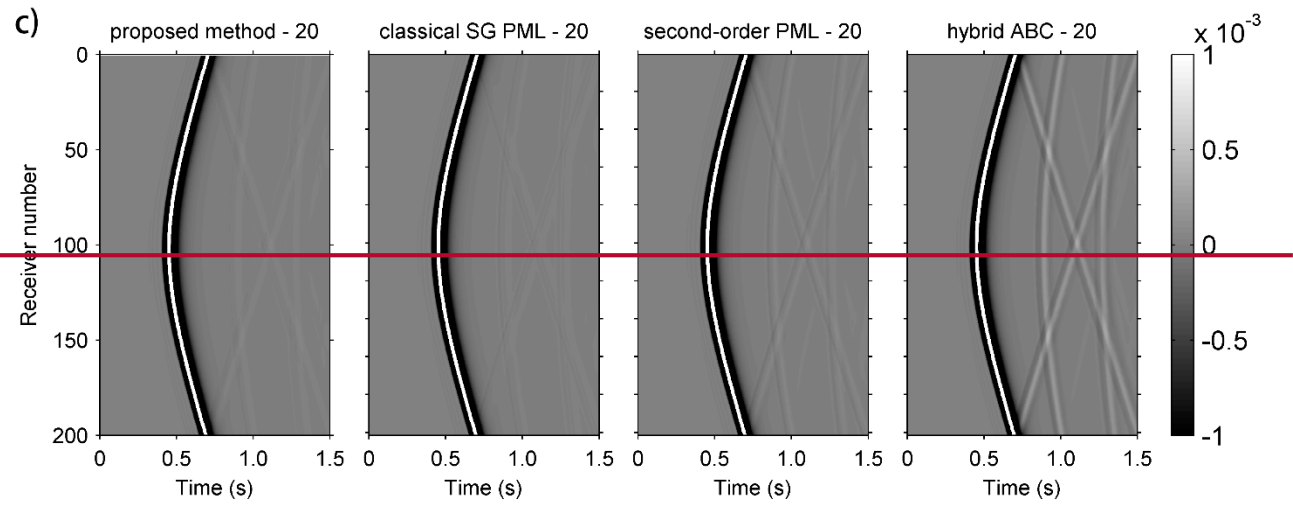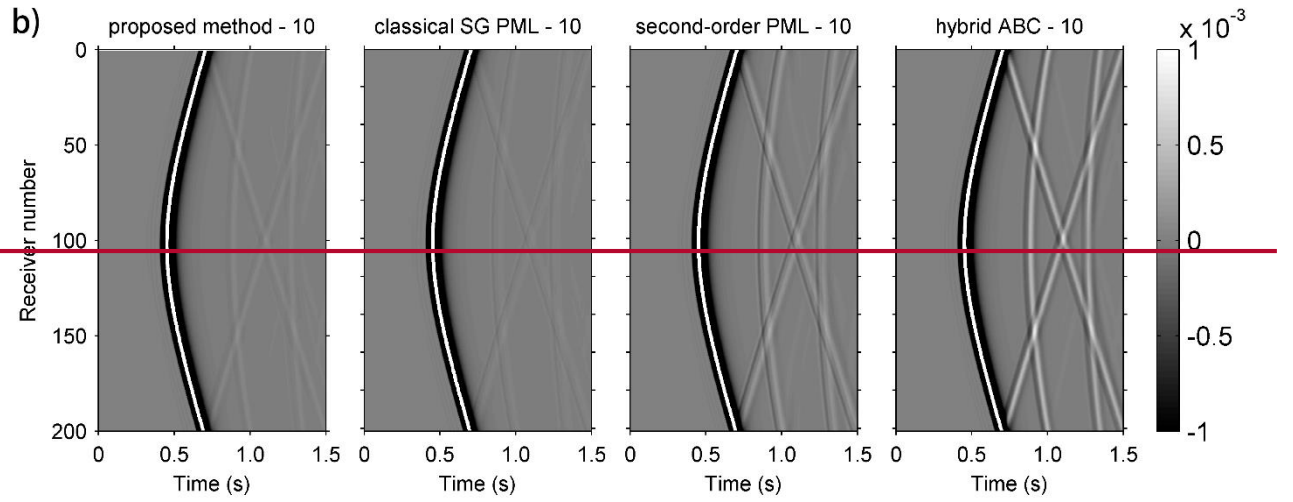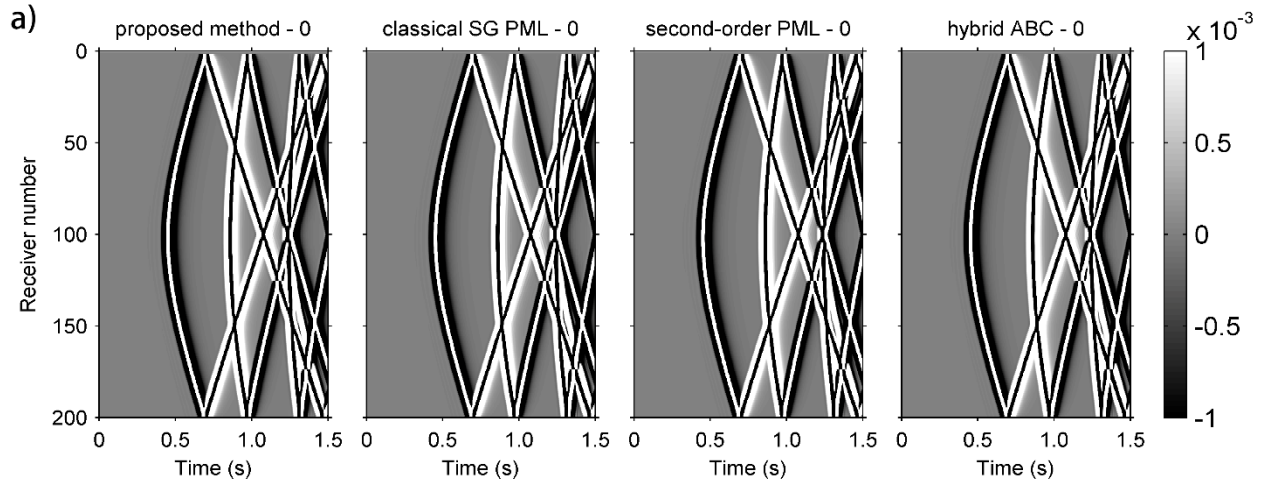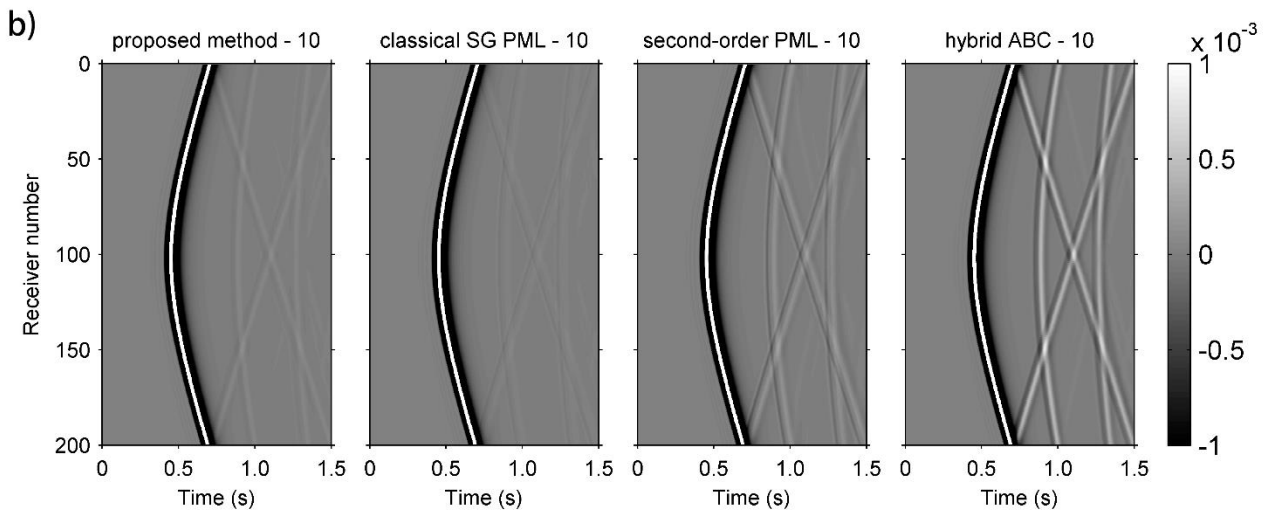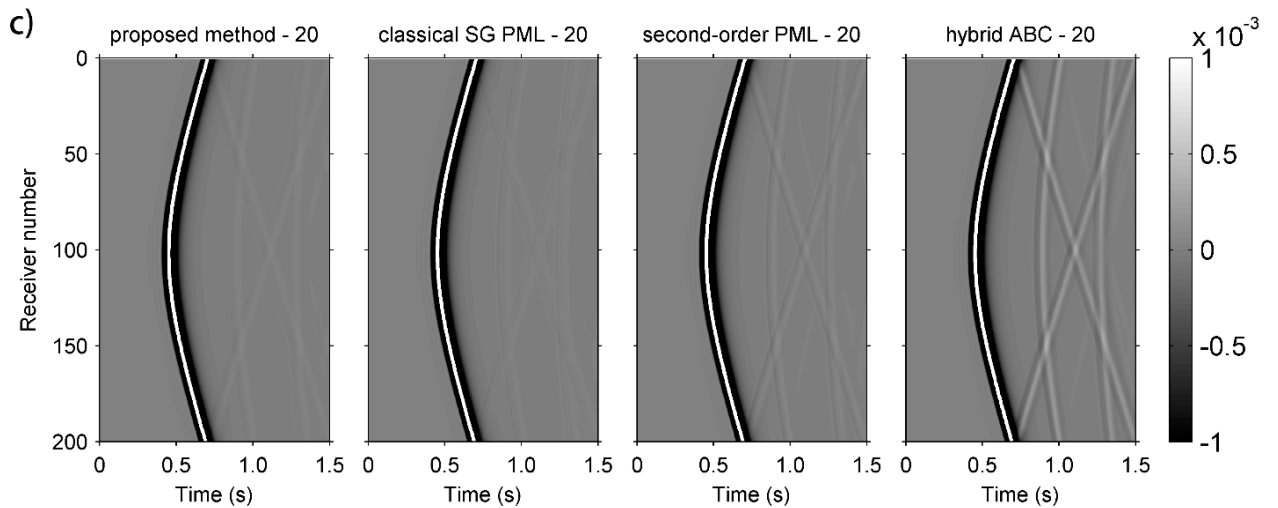
Figure 12. Receiving point records of the four methods for a different number of absorbing layers: (a) 0 absorbing layers; (b) 10 absorbing layers; and (c) 20 absorbing layers.
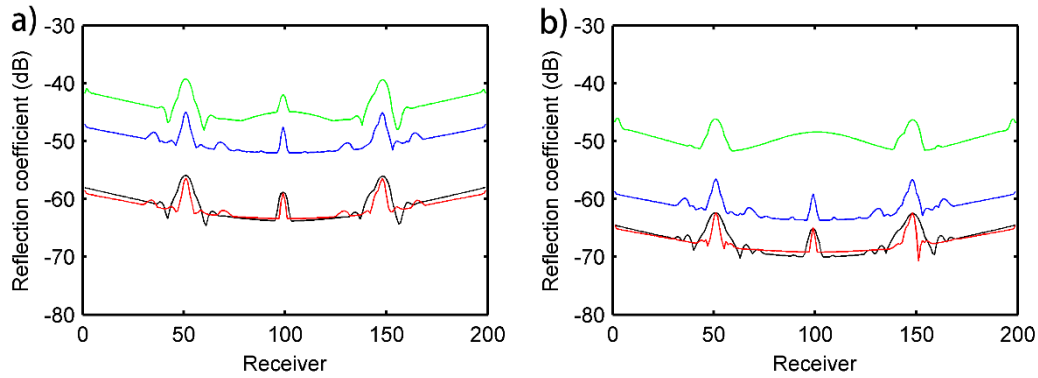
Figure 13. Values of the absorption coefficient R at each receiving point for our method (red line), the classic SG PML method (black line), the second-order PML method (blue line), and the hybrid ABC method (green line): (a) 10 absorbing layers; and (b) 20 absorbing layers.

As can be seen in Fig. 12 and 13, all of the four methods can absorb the reflected waves to a certain degree. For the same number of absorbing layers, the absorption performance of our method and that of the classic SG PML method are almost the same and both methods are superior to the other two methods, while the hybrid ABC method is the worst. Specifically, when the number of absorbing layers equals 10, the absorption coefficients of our method and classic SG PML method are both -60 dB, which means that the amplitude of the reflected wave after absorbing is only 0.1% of that before absorbing. Increasing the number of absorbing layers can improve the absorption effect of the four methods. In addition, the 20-layer, second-order PML method performs similarly to the 10-layer proposed method and the 10-layer classic SG PML method. This indicates that the second-order PML method always requires more absorbing layers than the first-order PML does. Although the core idea of the second-order PML method is the same as the first-order PML method, there are very different ways to deal with mathematical equations. In the second-order method, the original PML equations are transformed and some additional nonphysical variables are added, which greatly reduces the efficiency of boundary conditions. Moreover, the second-order PML method still need to handle the first-order system, i.e. an Euler or a Runge-Kutta time scheme has to be used (Komatitsch and Tromp, 2003). So in this case, the second-order PML method is naturally less effective than our first-order PML method and requires more absorbing layers. For hybrid ABC, it has poor absorbing performance than the PML method since it is based on a one-way equation. So it would have limited improvement due to the phase and the amplitude errors that are associated with the expansion of one-way wave equation.

4.2.1 Constant-gradient velocity model

Taking into account the fact that the homogeneous model is relatively simple and is quite different from the actual distribution of an underground medium, the second model that we use, is the constant-gradient velocity model, as shown in Fig. 14. The velocity is 1500 m/s at $z = 0$ m and 3500 m/s at $z = 2000$ m, and the velocity gradient is 1. The source and receiving point locations are exactly the same as those in the first homogeneous model. Figure 15 and 16 compare the receiving point records and the reflection coefficients R of the four methods for different boundary conditions. It can be seen that the absorption effect of this model is not as good as that of the homogeneous model, but the results are the same. For the same number of absorbing layers, our method has the same absorbing ability as that of the classic SG PML and performs better than the

1 other two methods. Also, we still need to use more layers for the second-order PML method instead of using

2 the thin method we proposed. In addition, we see that the 10-layer proposed method is much better than the 20-

3 layer hybrid ABC method.
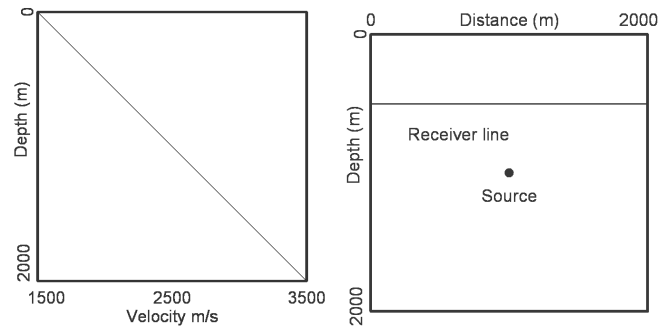
5 **Figure 14.** Velocity profiles with depth and the location of the source and receiving points.

a)

b)

c)
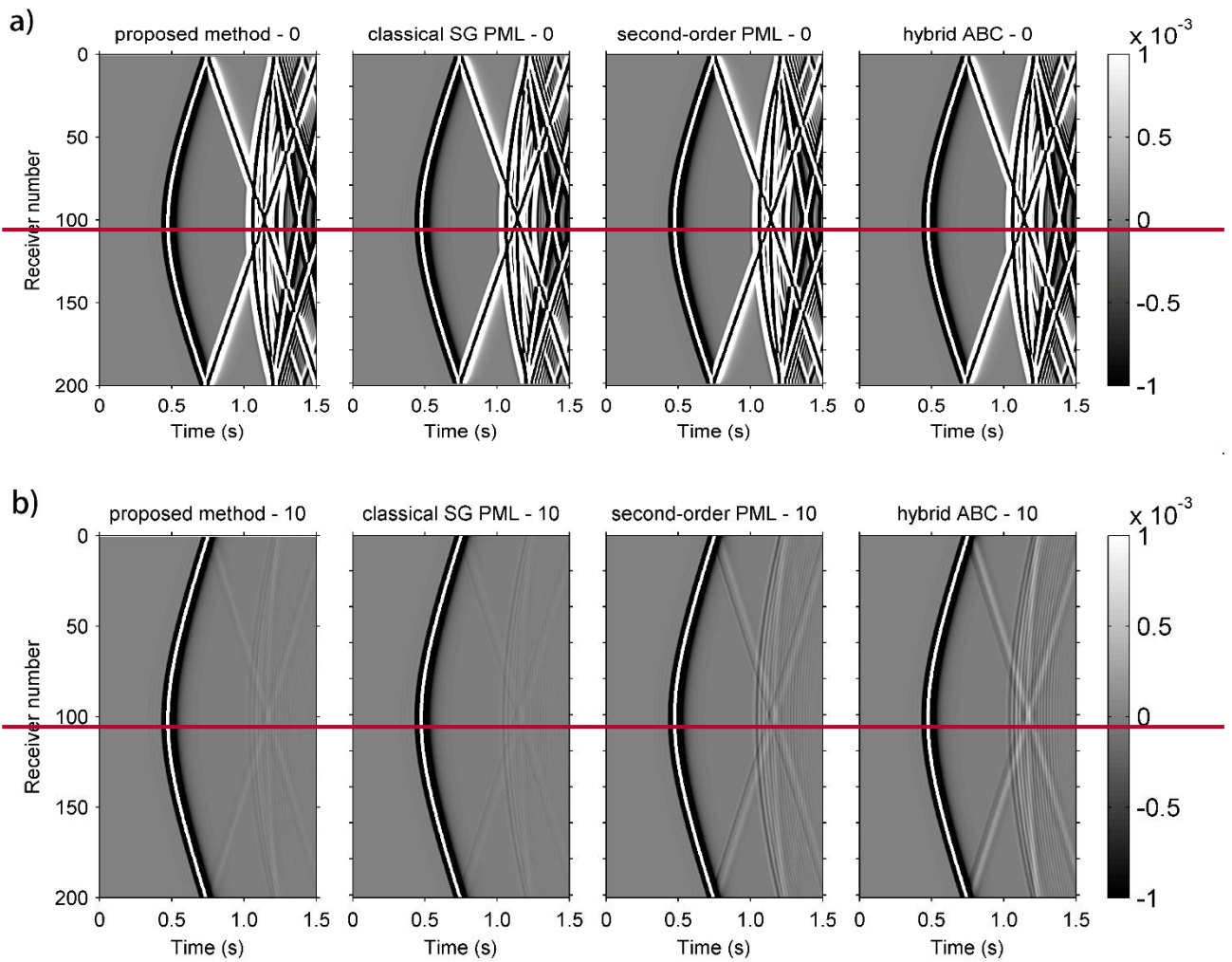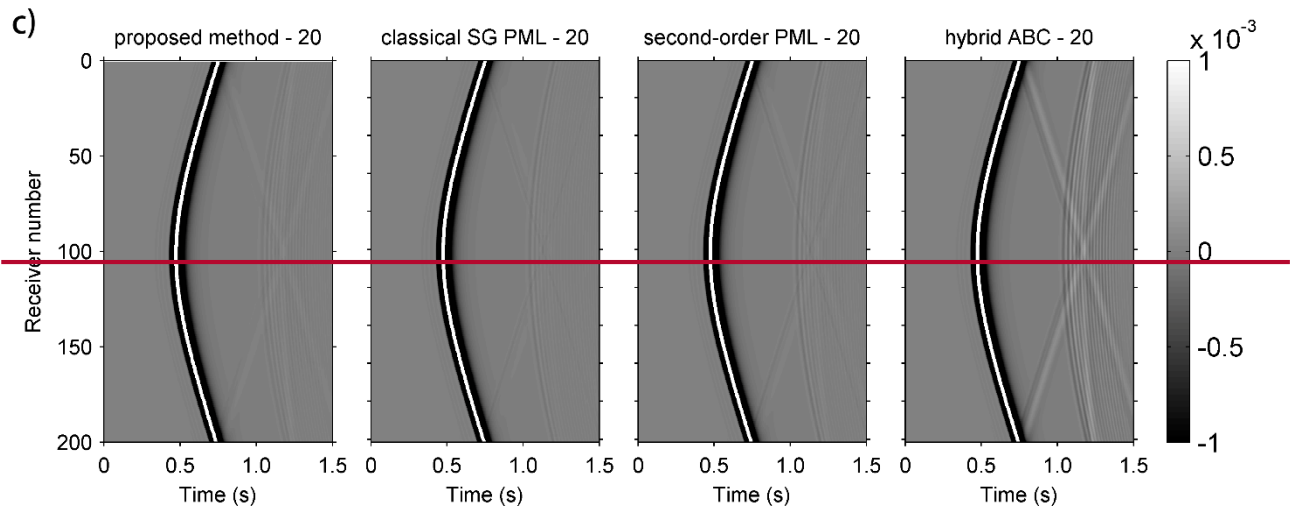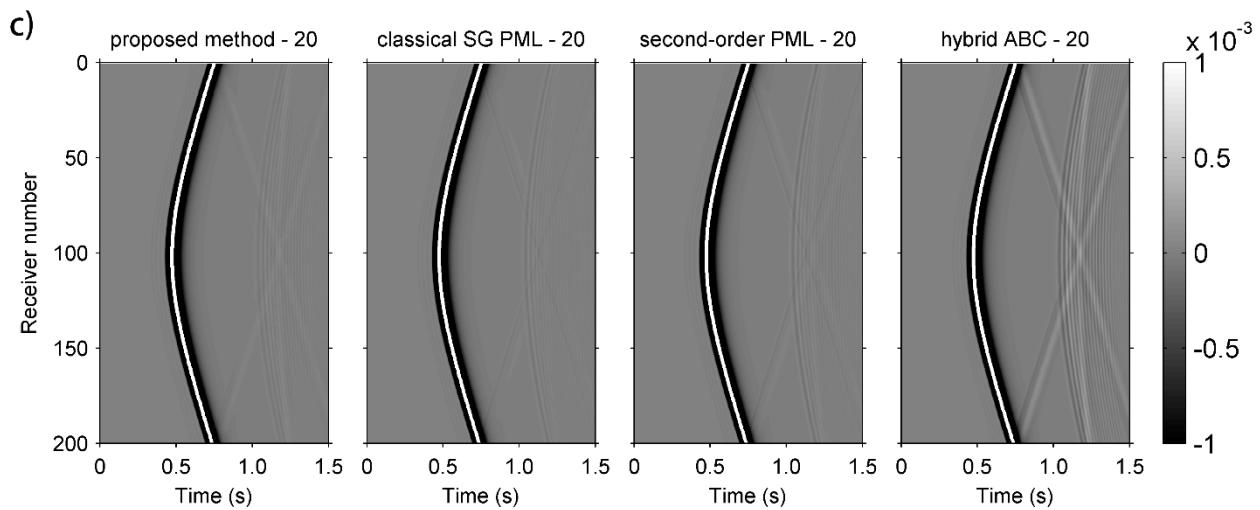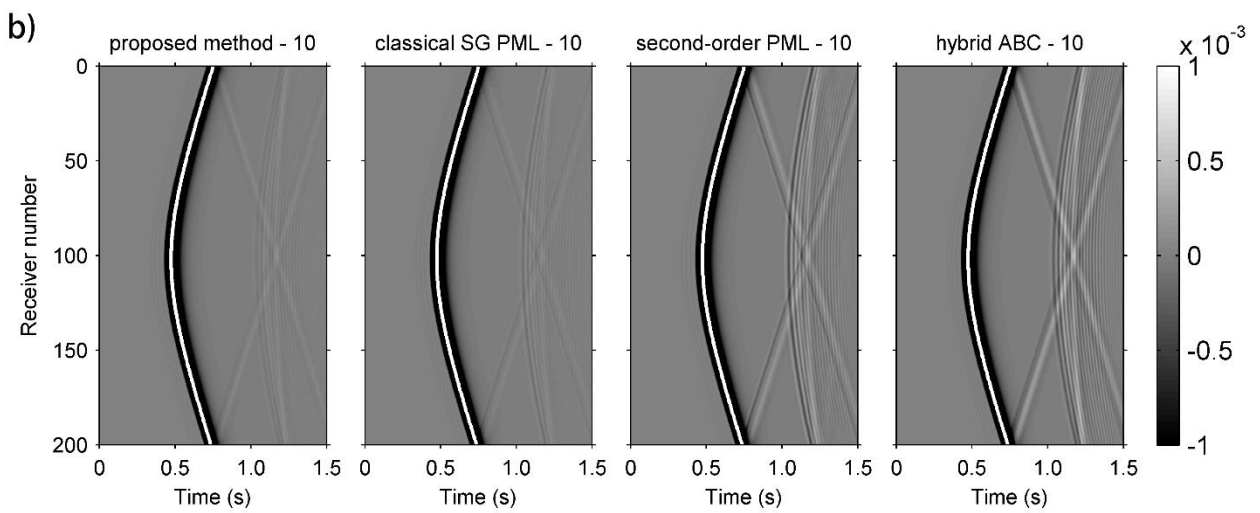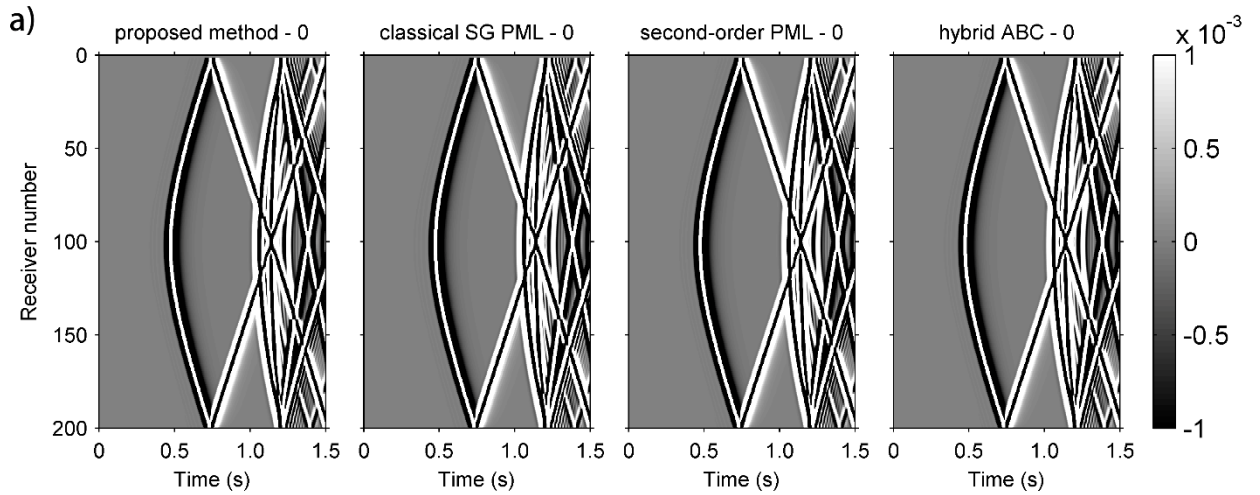
Figure 15. Receiving point records for the four methods for a different number of absorbing layers: (a) 0 absorbing layers; (b) 10 absorbing layers; and (c) 20 absorbing layers.
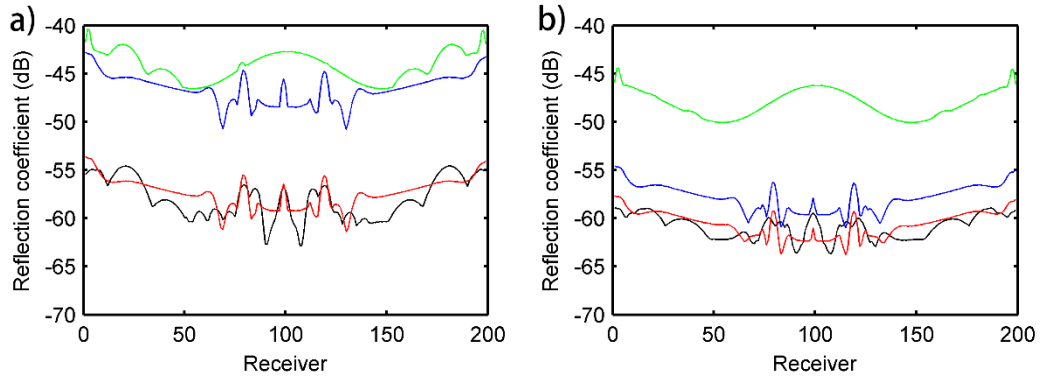
2 **Figure 16.** Values of the absorption coefficient R at each receiving point for our method (red line), the

3 classic SG PML method (black line), the second-order PML method (blue line), and the hybrid ABC method

4 (green line): (a) 10 absorbing layers; and (b) 20 absorbing layers.

5 4.2.3 Marmousi model

6 We next compared the absorption efficiency of the four methods for a complex Marmousi model. The

7 Marmousi model has a size of 9200 m×3000 m, a grid spacing of 12.5 m, a time step of 0.001 s, and a total

8 recording time of 8 s. The velocity distribution is shown in Fig. 17. Taking the first shot of the Marmousi model

9 as an example, we can see that the shot is located on the ground surface at a horizontal distance of 3000 m and

10 that the 185 receiving points are evenly distributed between 0–9200 m on the surface. The results in Fig. 18

11 show that the absorption effect of our method is equal to or better than the absorption effect of the other methods.

12 When the number of PMLs is 20, the reflected wave is relatively small. Therefore, the method we propose is

13 also suitable for simulating complex models.
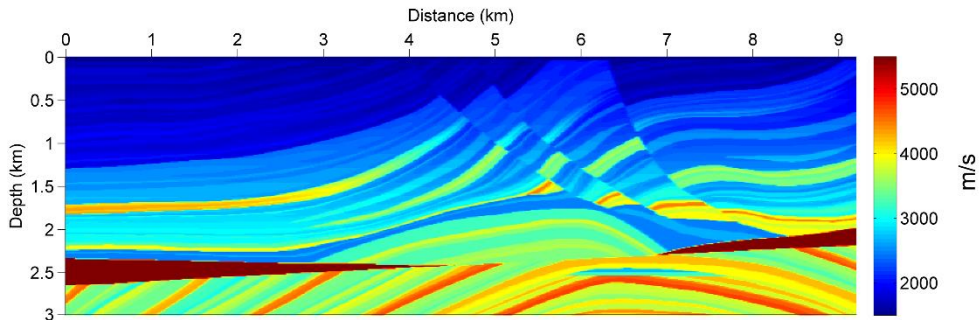
15 **Figure 17.** Marmousi velocity model
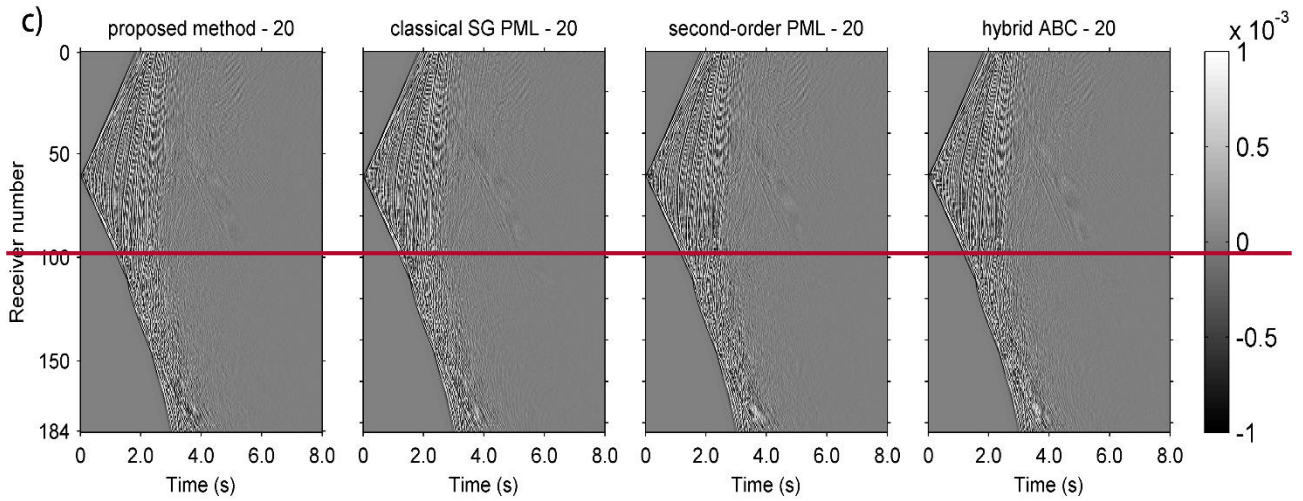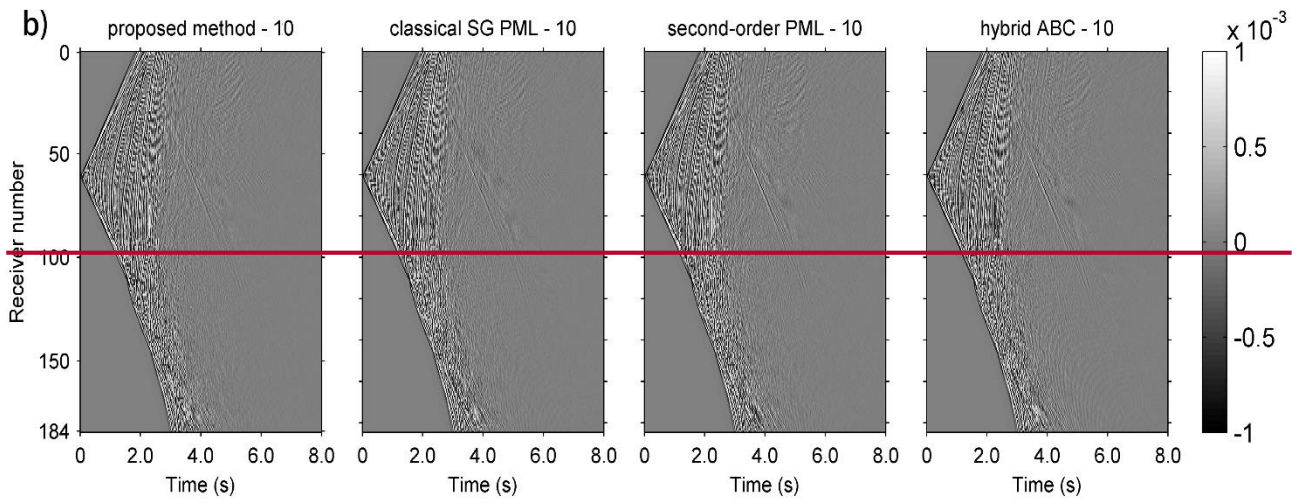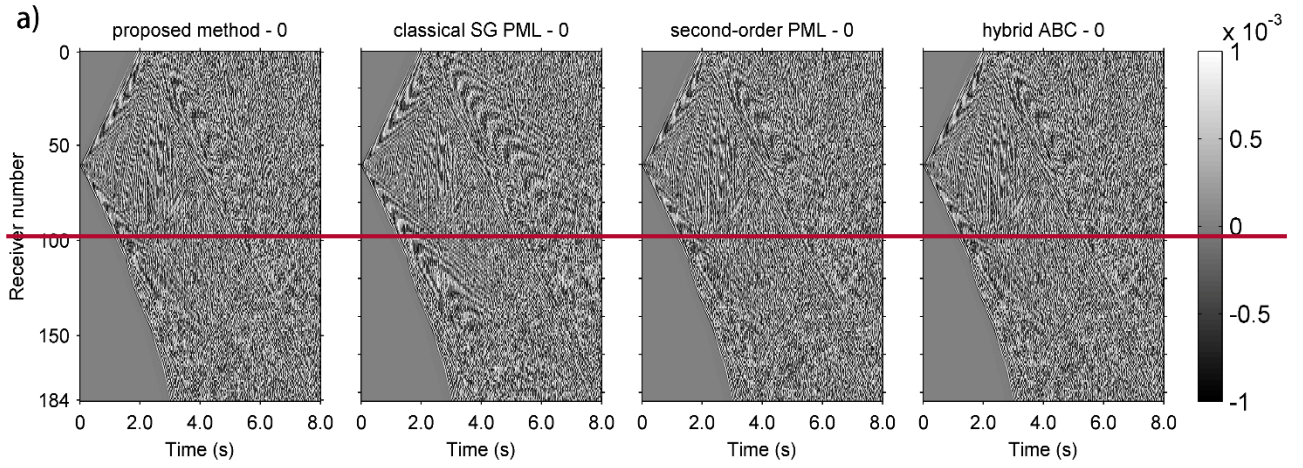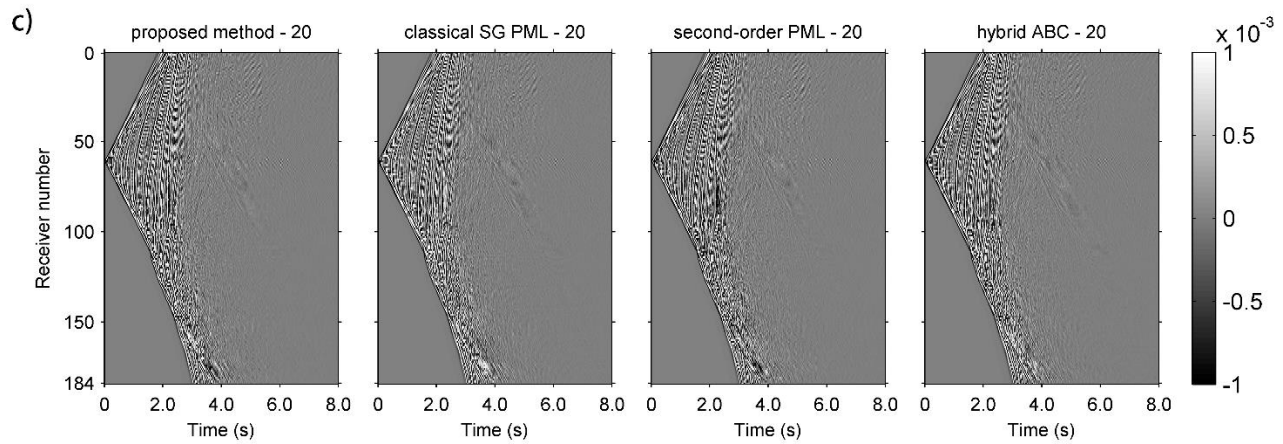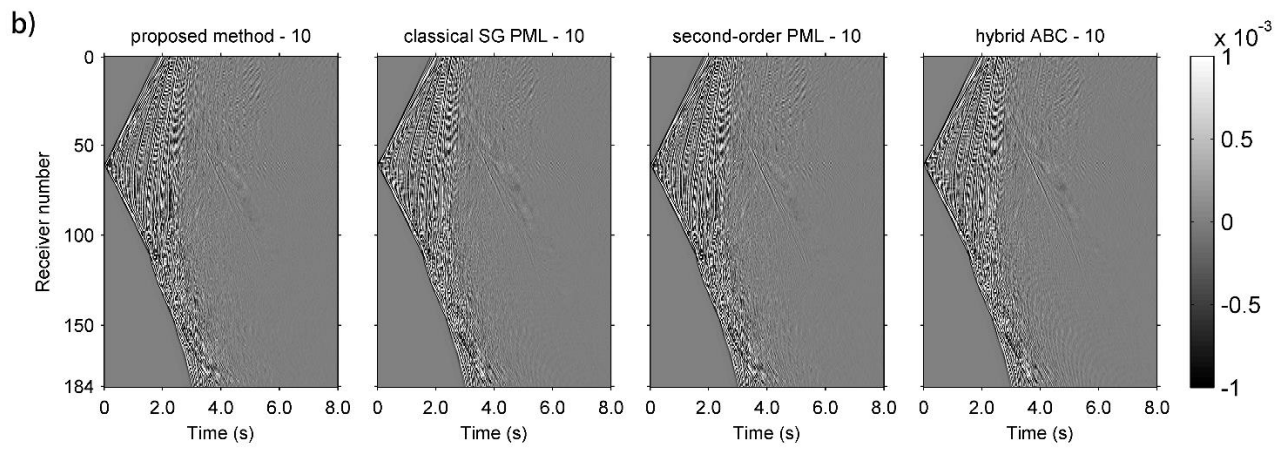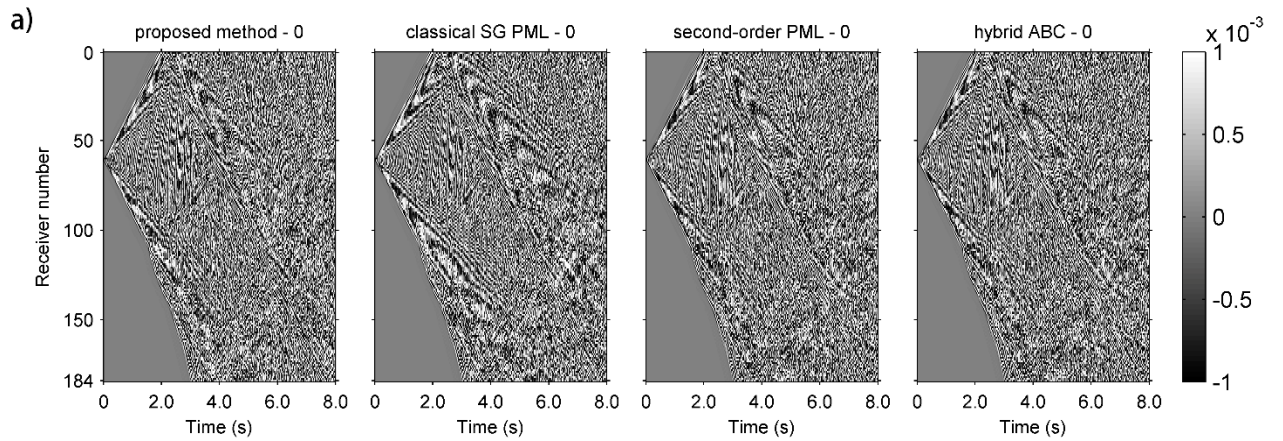
Figure 18. Receiving point records for the four methods for a different number of absorbing layers: (a) 0 absorbing layers; (b) 10 absorbing layers; and (c) 20 absorbing layers.

Based on the above numerical experiments, although the hybrid ABC method is often used as the boundary condition of the CG-based method because it is easy to deduce its second-order form, its absorption performance is obviously worse than those of the other three PML methods since it is based on a one-dimensional wave equation. Among the three PML methods, the 10-layer classic SG PML method (first-order PML is used inside) for the first-order wave equation is enough to suppress the edge reflections, while the 20-layer second-order PML method is sufficient for the second-order wave equation. However, our first-order PML method only requires a thickness of 10 grid spacings to absorb the outgoing wave entirely. It may have a significant

advantage over the second-order PML method. Table 2 shows the computation times of the four methods for different numbers of absorbing layers. Among them, the computation time of our method is the shortest and that of the classic SG PML method is the longest. Given that our method uses the CG scheme in the computational area, it requires much less computation time than the classic SG PML method does. In addition, the second-order PML method requires the transformation of the original first-order PML equation into a second-order form. The required complex formulas and extra variables without physical meaning increase the computation time. In addition, our method naturally implements high-order temporal discretization if necessary, while the second-order PML method does not. Therefore, our method is ideal for seismic wave forward modeling.

Table 2. Computation times for the four methods.

Condition	Our method	Classic SG PML method	Second-order PML method	Hybrid ABC method
homogeneous model PML=10	20 sec	28 sec	24 sec	20 sec
homogeneous model PML=20	24 sec	34 sec	28 sec	25 sec
constant-gradient velocity model PML=10	21 sec	30 sec	26sec	21 sec
constant-gradient velocity model PML=20	25 sec	35 sec	30 sec	26 sec
Marmousi model PML=10	6 m 57 sec	10 m 31 sec	8 m 20 sec	7 m 14 sec
Marmousi model PML=20	6 m 05 sec	9 m 05 sec	7 m 18 sec	6 m 25 sec

4.3 Three-dimensional homogeneous model

In order to facilitate the experiments and comparative analyses, we used the two-dimensional models described in the above numerical experiments. To further illustrate the effectiveness of our method, Fig. 19 shows the experimental results of this method for a three-dimensional homogeneous velocity model. The model size is 1000 m×1000 m×1000 m, the grid spacing is 10 m, and the velocity is 2000 m/s. The source is located at (500 m, 500 m, 500 m) with a time step of 0.001 s. Figure 19 shows snapshots of the wave field at different times. From this we find that when the number of PMLs is 20, the wave field record is very clear, and almost no reflected waves are seen.
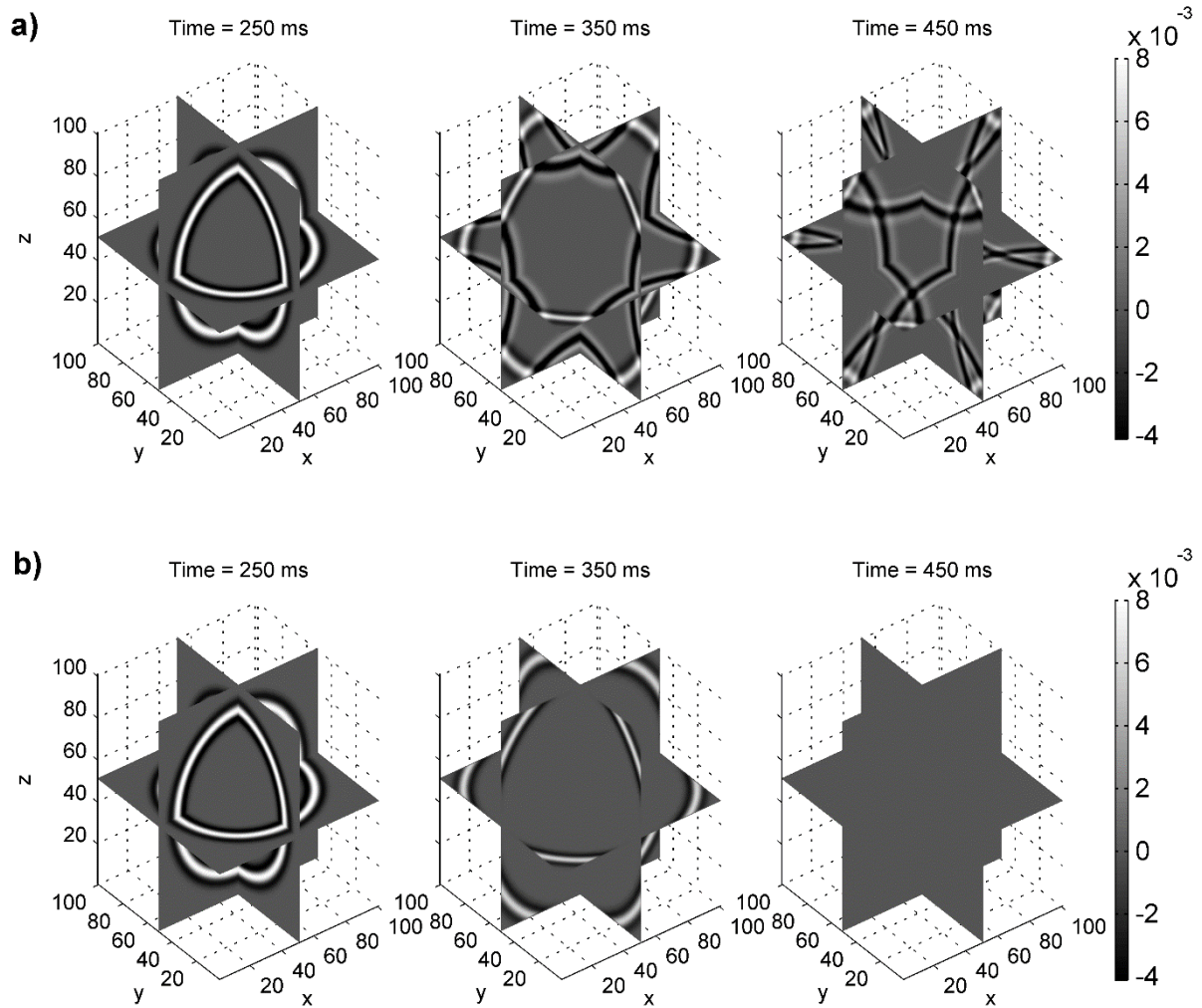
3   **Figure 19.** Wave field snapshots with different PML at different time, the three coordinate axis represent
4 the number of grids in three directions.: (a) PML=0 at 250 ms, 350 ms and 450 ms; (b) PML=20 at 250 ms, 350
5 ms and 450 ms.

6   5. Conclusions

7   We propose a new boundary matched algorithm that effectively combines the CG scheme in the
8 computational area and the SG scheme in the PML boundary conditions, while preserving the high
9 computational efficiency of the CG scheme and the good absorption effect of PML boundary conditions. Our
10 proposed method is easy to implement, and we only perform appropriate wave field matching at the grid points,
11 which avoids ~~complex~~complicated modifications to the PML formulas and the ~~addition~~introduction of
12 unnecessary variables. The numerical experiments of the different models indicate that our method is ~~suitable~~
13 ~~for use with~~applicable to a variety of simple and complex two-dimensional and three-dimensional geological
14 models. For the same conditions, our method can achieve similar or better accuracy and reflected wave
15 absorption efficiency as other boundary absorption methods, ~~but~~while it requires less computation time.
16 Because our method ~~preserves~~keeps the independence of the computational area and the boundary absorption
17 area, it can also be ~~used~~combined with other CG-based seismic wave numerical algorithms, such as the nearly

analytical center difference method with PML boundary conditions, to achieve better numerical simulation accuracy.

Our work is based on the numerical simulation of a scalar equation. Because the elastic wave equation includes more wave field information, it is also widely used in the numerical simulation of seismic waves. The simulation of the elastic wave equation requires more computations and greater storage capacity, while our proposed method ~~has a small~~can reduced the computational cost. ~~After being properly modified,~~The next step of our ~~method can~~work will be ~~used for~~ the numerical simulation of the elastic wave equation and is expected to significantly improve its computational efficiency~~, which is the next step in our work~~.

Acknowledgments:

This research work was financially supported by the National Science and Technology Major Project of China under Grant 2011zx05003-003.

References

Alford, R. M., Kelly, K. R. and Boore, D.: Accuracy of finite-difference modeling of the acoustic wave equation, Geophysics, 39, 834-842, 1974.

Berenger, J. P.: A Perfect Matched Layer for the Absorption of Electromagnetic Waves, Journal of Computational Physics, 114, 185-200, 1994.

Blanch, J. O. and Robertsson, J. O. A.: A modified Lax-Wendroff correction for wave propagation in media described by Zener elements, Geophysical Journal of the Royal Astronomical Society, 131, 381-386, 2010.

Cerjan, C., Kosloff, D., Kosloff, R. and Reshef, M.: A nonreflecting boundary condition for discrete acoustic and elastic wave equations, Geophysics, 50, 705-708, 1985.

Cerveny, V.: Seismic ray theory, Cambridge University Press, 2001.

Chew, W. C. and Liu, Q. H.: Perfectly matched layers for elastodynamics: a new absorbing boundary condition, Journal of Computational Acoustics, 4, 341-359, 1996.

Chu, C. L. and Stoffa, P. L.: Determination of finite-difference weights using scaled binomial windows. 2012 Geophysics, 77, W17-W26, 2012.

Clayton, R. and Engquist, B.: Absorbing boundary conditions for acoustic and elastic wave equations. Bull.seism.soc.am, 67, 1529-1540, 1977.

Collino, F. and Tsogka, C.: Application of the perfectly matched absorbing layer model to the linear elastodynamic problem in anisotropic heterogeneous media, Geophysics, 66, 294-307, 1998.

Dablain, M. A.: The application of high-order differencing to the scalar wave equation. Geophysics, 51, 54, 1986.

Dan, D. K. and Baysal, E.: Forward modeling by a Fourier method. Geophysics, 47, 1402-1412, 1982.

Engquist, B. and Runborg, O.: Computational high frequency wave propagation, Acta Numerica, 12, 181-266, 2003.

Fornberg B.: High-Order Finite Differences and the Pseudospectral Method on Staggered Grids, Siam Journal on Numerical Analysis, 27, 904-918, 1990.

Gao, Y. J., Song, H., Zhang, J. and Yao, Z.: Comparison of artificial absorbing boundaries for acoustic wave equation modelling, Exploration Geophysics, 48, 76-93, 2017.

Gold, N., Shapiro, S. A. and Burr, E.: Modelling of high contrasts in elastic media using a modified finite difference scheme. Seg Technical Program Expanded, 1850-1853, 1997.

Grote, M. J. and Sim, I.: Efficient PML for the wave equation, Mathematics, 2010.

Higdon, R. L.: Absorbing boundary conditions for elastic waves: Siam Journal on Numerical Analysis, 31, 64-100, 2012.

Huang, C. and Dong, L.: Staggered-Grid High-Order Finite-Difference Method in Elastic Wave Simulation with Variable Grids and Local Time Steps, Chinese Journal of Geophysics, 52, 1324–1333, 2009.

Hustedt, B., Operto, S. and Virieux, J.: Mixed-grid and staggered-grid finite-difference methods for frequency-domain acoustic wave modelling, Geophysical Journal of the Royal Astronomical Society, 157, 1269-1296, 2004.

Igel, H., Mora, P. and Riollet, B.: Anisotropic wave propagation through finite-difference grids, Geophysics, 60, 1203-1216, 1995.

Kelly, K. R., Ward, R. W. Treitel, S. and Alford, R. M.: Synthetic seismograms: a finite-difference approach, Geophysics, 41, 2-27, 2012.

Komatitsch, D. and Tromp, J.: A perfectly matched layer absorbing boundary condition for the second-order seismic wave equation, Geophysical Journal International, 154, 146–153, 2003.

Komatitsch, D. and Martin, R.: An unsplit convolutional perfectly matched layer improved at grazing incidence for the seismic wave equation, Geophysics, 72, SM155-SM167, 2007.

Kreiss, H. O. and Oliger, J.: Comparison of accurate methods for the integration of hyperbolic equations, Tellus, 24, 199-215,1972.

Lax, P. D. and Wendroff, B.: Difference schemes for hyperbolic equations with high order of accuracy. Communications on Pure & Applied Mathematics, 17, 381-398, 1964.

Li, B., Liu, Y., Sen, M. K. and Ren, Z.: Time-space-domain mesh-free finite difference based on least squares for 2D acoustic-wave modeling, Geophysics, 82, 143-157, 2017.

Liu, Q. H. and Tao, J.: The perfectly matched layer for acoustic waves in absorptive media, Journal of the Acoustical Society of America, 102, 2072-2082, 1998.

Liu, Y. and Sen, M. K,: Scalar Wave Equation Modeling with Time-Space Domain Dispersion-Relation-Based Staggered-Grid Finite-Difference Schemes, Bull.seism.soc.am, 101, 141-159, 2011.

Madariaga, R.: Dynamics of an expanding circular fault, Bull.seism.soc.am, 66, 639-666, 1976.

Marfurt, K. J.: Accuracy of finite-difference and finite-element modeling of the scalar and elastic wave equations, Geophysics, 49, 533-549, 1987.

Moczo, P. Robertsson, J. O. A. and Eisner, L.: The Finite-Difference Time-Domain Method for Modeling of Seismic Wave Propagation, Advances in Geophysics, 48, 421-516, 2007.

Moczo, P., Kristek, J., Galis, M., Chaljub, E. and Etienne, V.: 3-D finite-difference, finite-element, discontinuous-Galerkin and spectral-element schemes analysed for their accuracy with respect to P-wave to S-wave speed ratio, Geophysical Journal International, 187, 1645–1667, 2011.

Moczo, P., Kristek, J. and Galis, M.: The finite-difference modelling of earthquake motions: waves and ruptures, Cambridge University Press, 1-365, 2014.

O'Brien, G. S.: 3D rotated and standard staggered finite-difference solutions to Biot's poroelastic wave equations: Stability condition and dispersion analysis, Geophysics, 75, 111-119, 2010.

Pasalic, D. and McGarry, R.: Convolutional perfectly matched layer for isotropic and anisotropic acoustic wave equations, 2010 SEG Annual Meeting. Society of Exploration Geophysicists, 2010.

Ren, Z. M. and Liu, Y.: A Hybrid Absorbing Boundary Condition for Frequency-Domain Visco-Acoustic Finite-Difference Modeling, Journal of Geophysics & Engineering, 10, 86-95, 2012.

Reynolds, A. C.: Boundary conditions for the numerical solution of wave propagation problems, Geophysics, 43, 155-165, 1978.

Saenger, E. H., Gold, N. and Shapiro, S. A.: Modeling the propagation of elastic waves using a modified finite-difference grid, Wave Motion, 31, 77-92, 2000.

Sánchez-Sesma, F. J. Madariaga, R. and Irikura, K.: An approximate elastic two-dimensional Green's function for a constant-gradient medium, Geophysical Journal International, 146, 237–248, 2001.

Sochacki, J, Kubichek, R., George, J., Fletcher, W. and Smithson, S.: Absorbing boundary conditions and surface waves, Geophysics, 52, 60-71, 1987.

Tan, S. R. and Huang, L.: A staggered-grid finite-difference scheme optimized in the time–space domain for modeling scalar-wave propagation in geophysical problems, Journal of Computational Physics, 276, 613-634, 2014.

Virieux, J.: SH-wave propagation in heterogeneous media: Velocity-stress finite-difference method, Geophysics, 49, 1933–1942, 1984.

Virieux, J.: P-SV wave propagation in heterogeneous media; velocity-stress finite-difference method, Geophysics, 49, 1933-1942, 1986.

Wang, S. D.: Absorbing boundary condition for acoustic wave equation by perfectly matched layer, Oil Geophysical Prospecting, 38, 31-34, 2003.

Yang, D. H., Teng, J. W., Zhang, Z. J. and Liu, E.: A nearly analytic discrete method for acoustic and elastic wave equations in anisotropic media, Bull.seism.soc.am, 93, 2389-2401, 2003.

Yang, D. H., Tong, P. and Deng, X.: A central difference method with low numerical dispersion for solving the scalar wave equation, Geophysical Prospecting, 60, 885–905, 2012.

Yang, D. Liu, E. Zhang, Z. J. and Teng, J.: Finite-difference modelling in two-dimensional anisotropic media using a flux-corrected transport technique, Geophysical Journal International, 148, 320-328, 2002.

Yang, D., Liu, E. and Zhang, Z.: Evaluation of the u-W finite element method in anisotropic porous media, Journal of Seismic Exploration, 17, 273-299. 2008.

Yang, L., Yan, H. and Liu, H.: Optimal rotated staggered-grid finite-difference schemes for elastic wave modeling in TTI media, Journal of Applied Geophysics, 122, 40-52, 2015.

Zhang, J. H. and Yao, Z. X.: Optimized finite-difference operator for broadband seismic wave modeling, Geophysics, 78, A13-A18, 2013.

Zhang, Z. G., Zhang, W., Li, H. and Chen, X.: Stable discontinuous grid implementation for collocated-grid finite-difference seismic wave modelling, Geophysical Journal International, 192, 1179-1188, 2013.